ACS OMEGA

Open Access

This article is licensed under CC-BY 4.0

http://pubs.acs.org/journal/acsodf

Article

In Silico Study of the Anti-MYC Potential of Lanostane-Type Triterpenes

José A. C. Oliveira, Jonatas M. Negreiro, Fátima M. Nunes, Francisco G. Barbosa, Jair Mafezoli, Marcos C. Mattos, Maria C. R. Fernandes, Claudia Pessoa, Cristiana L. M. Furtado, Geancarlo Zanatta,* and Maria C. F. Oliveira*

Cite This: *ACS Omega* 2024, 9, 50844−50858

Read Online

ACCESS | Metrics & More | Article Recommendations | Supporting Information

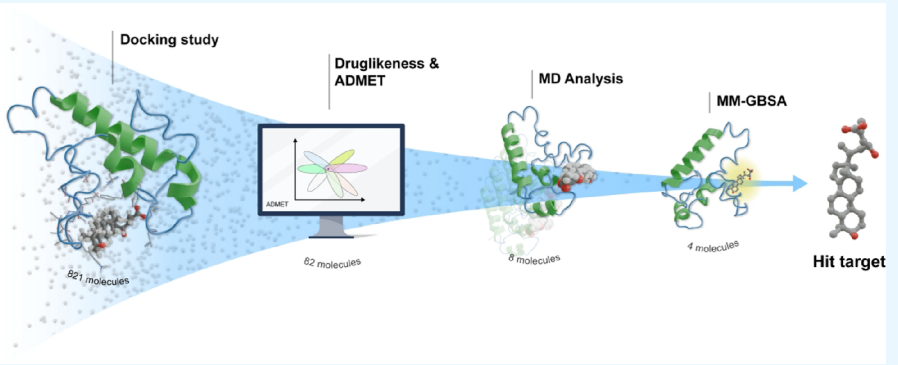

ABSTRACT: One of the most investigated molecular targets for anticancer therapy is the proto-oncogene *MYC*, which is amplified and thus overexpressed in many types of cancer. Due to its structural characteristics, developing inhibitors for the target has proven to be challenging. In this study, the anti-MYC potential of lanostane-type triterpenes was investigated for the first time, using computational approaches that involved ensemble docking, prediction of structural properties and pharmacokinetic parameters, molecular dynamics (MD), and binding energy calculation using the molecular mechanics-generalized born surface area (MM-GBSA) method. The analysis of physicochemical properties, druglikeness, and pharmacokinetic parameters showed that ligands ganoderic acid E (**I**), ganoderlactone D (**II**), ganoderic acid Y (**III**), ganoderic acid Df (**IV**), lucidenic acid F (**V**), ganoderic acid XL_4 (**VI**), mariesiic acid A (**VII**), and phellinol E (**VIII**) presented properties within the filter used. These eight ligands, in general, could interact with the molecular target favorably, with interaction energy values between −8.3 and −8.6 kcal mol^{-1}. In MD, the results of RMSD, RMSF, radius of gyration, and hydrogen bonds of the complexes revealed that ligands **I**, **IV**, **VI**, and **VII** interacted satisfactorily with the protein during the simulations and assisted in its conformational and energetic stabilization. The binding energy calculation using the MM-GBSA method showed better results for the MYC-**VII** and MYC-**I** complexes (−44.98 and −41.96 kcal mol^{-1}, respectively). These results support the hypothesis that such molecules can interact with MYC for a considerable period, which would be an essential condition for them to exert their inhibitory activity effectively.

INTRODUCTION

The MYC (also known as C-MYC) protein is a transcriptional factor belonging to the basic helix−loop−helix zipper (bHLHZiP) family, which plays important roles in regulating gene expression influencing fundamental cellular processes, such as growth, proliferation, differentiation, and cell death.[1−4] MYC is a proto-oncogene that is highly expressed during embryonic development and becomes inactivated in adult somatic cells.[5,6] However, oncogenic activation and overexpression of the MYC family are reported in many malignant neoplasms, making it one of the most investigated molecular targets in anticancer therapy.[6−9] Genomic alterations, epigenetic modifications, and post-translational protein remodeling are associated with MYC activation in human cancers.

MYC overexpression is often associated with gene amplification and chromosomal rearrangements.[10] Additionally, genetic variants, such as point mutations and indels (insertions/deletions), can enhance MYC protein stability and activity contributing to cancer progression.[11] Increased

Received: November 9, 2024
Revised: November 30, 2024
Accepted: December 5, 2024
Published: December 12, 2024

© 2024 The Authors. Published by American Chemical Society

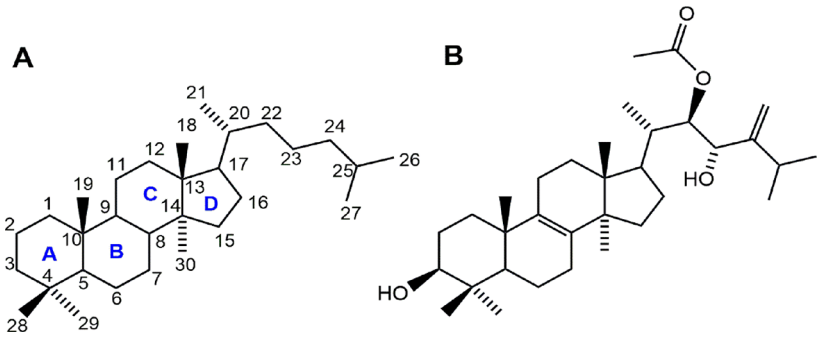

Figure 1. Chemical structures of the lanostane-type triterpene skeleton (A) and pisosterol (B).

enhancer activity or the activation of superenhancers surrounding the MYC locus through mechanisms like chromosomal translocations or retroviral promoter insertion can lead to constitutive activation of MYC expression driving carcinogenesis.[12] Furthermore, aberrant epigenetic reprogramming, such as the loss of DNA methylation, dysregulated noncoding RNA expression, and changes in histone marks, has been reported to activate the *MYC* proto-oncogene.[13] Post-translational modification, such as phosphorylation at S62 and *trans*−*cis*-prolyl-isomerization at P63, stabilizes and activates the MYC protein. Arginine methylation of MYC protein has also been suggested to alter its stability.[14]

The *MYC* oncogene has been identified in approximately 75% of all aggressive cancers and is related to low response to available conventional therapies.[5,15] The mechanisms by which *MYC* is related to cancer development have not yet been fully elucidated. However, it is known that its oncogenic effects occur, in part, through association with MAX (MYC-associated factor X) protein. The heterodimer MYC-MAX binds to promoter regions of target genes involved in cell growth, proliferation, and metabolism contributing to oncogenic effects of MYC.[16−20] Many challenges are faced in developing MYC inhibitors, as this protein has an intrinsically disordered chemical structure manifesting itself in a dynamic range of unstable conformations devoid of effective sites on its surface.[21] Due to these characteristics, the molecular target was considered undruggable for a long time.[21−23] Despite the obstacles, many prototype direct and indirect inhibitors have been designed or are in development.[24−34] Furthermore, computational methods have also helped the discovery and development of bioactive molecules and enabled the screening of thousands of compounds aiming to identify inhibitors for MYC or MYC-MAX.[35−41] Until now, only a few small molecules and peptide inhibitors have been reported, and all have demonstrated failures in clinical trials due to their inadequate pharmacokinetic behavior and lack of efficacy under *in vivo* conditions.[40]

In this context, natural products can be investigated as potential bioactive compounds with anti-MYC potential. Among the bioactive natural compounds reported in the literature, lanostane-type triterpenes are molecules biosynthesized by living organisms via the mevalonate pathway.[42] They are mainly produced by fungi of the genus *Ganoderma* and have diverse structural characteristics that are still being explored.[43,44] Lanostane triterpenes can have chemical structures with 24, 27, or 30 carbon atoms. The standard skeleton (Figure 1A) is formed by the junction of four rings with trans configurations A/B, B/C, and C/D and may present substituents mainly in positions C-3, C-7, C-11, C-12, C-15, C-22, C-23, C-24, and C-25.[45] Major related activities include anticancer, anti-HIV, antinociceptive, antimicrobial, anti-AchE, antiviral, antimalarial, and anti-inflammatory.[46−53]

The anticancer potential of pisosterol (Figure 1B), a lanostane-type triterpene produced by the basidiomycete *Pisolithus tinctorius*, has been studied by our group. The cytotoxic effect of this compound was investigated in three animal cell models.[54] Pisosterol did not show relevant cytotoxicity in mouse erythrocytes or sea urchin embryos but showed selectivity for inhibiting the growth of the tumor cell lines SF-268 (human neuroblastoma), B16 (murine melanoma), PC-3 (human prostate cancer), MCF-7 (human breast cancer), HCT-8 (human colon cancer), HL-60 (human leukemia), and CEM (human leukemia), especially for leukemia and melanoma cells (IC_{50} of 1.55, 1.84, and 1.65 $\mu g\ mL^{-1}$ for CEM, HL-60, and B16, respectively).

Another study evaluated the effects of pisosterol on the viability of HL-60 cells over time and at different doses. As a result, a significant drop in cell viability was observed due to the increase in exposure time and concentration of pisosterol, with notable reductions of up to 80% after 72 h at 5.0 $\mu g\ mL^{-1}$. The study also highlighted the ability of this triterpene to cause morphological changes in the cytoplasm of these cells.[55]

The *in vivo* study conducted by our research group confirmed the antitumor activity of pisosterol in mice with Sarcoma 180 when they were administered at doses of 50 or 100 mg m^{-2}. The percentage of inhibition of tumor growth for the mentioned doses presented rates of 43.0 and 38.7%, respectively. Histopathological analysis to investigate possible toxicity effects showed that the liver and kidney were the main organs affected by pisosterol, although such changes were considered reversible.[56]

Our group also performed a morphological and cytogenetic study using fluorescence *in situ* hybridization analysis of the locus for MYC in two HL-60 cell lines before and after treatment with pisosterol. It was found that at a dose of 1.8 $\mu g\ mL^{-1}$, around 15% of the cells showed stained regions, and 39.5% showed few fluorescence signals (3 or 4 alleles), showing that the triterpene probably blocks cells with stained regions in the interphase.[57] The same behavior was observed for glioblastoma multiforme cells (U343 and AHOL1). Before treatment, 72% of U343 cells and 65% of AHOL1 cells contained more than two *C-MYC* alleles. Pisosterol, when tested at a concentration of 1.8 $\mu g\ mL^{-1}$, was able to block gene amplification, as only 33% of U343 cells and 15% of AHOL1 cells showed more than two fluorescence signals.[58]

The antitumor potential of pisosterol, besides the lack of computational studies on the anti-MYC potential of natural

https://doi.org/10.1021/acsomega.4c10201
ACS Omega 2024, 9, 50844−50858

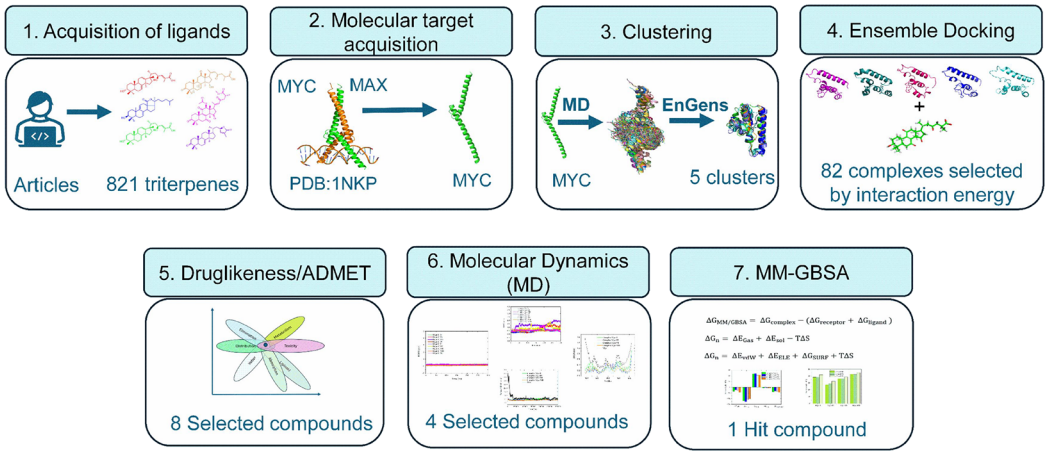

Figure 2. Workflow employed in the study.

products, motivated us to investigate 821 lanostane-type triterpenes as MYC inhibitors using computational methods.

RESULTS AND DISCUSSION

The workflow (Figure 2) employed in this study involved structure-based virtual screening using molecular docking studies, prediction of physicochemical (druglikeness) and pharmacokinetic properties, MD simulations, and binding energy calculation using the MM-GBSA method.

Construction of the Conformational Ensemble. The disordered nature of the MYC protein has been an obstacle to the design of new inhibitors.[38] Due to the high conformational complexity of this molecular target, it became necessary to build a conformational set of relatively stable structures to improve the chances of ligand coupling. Knowing this, a 400 ns MD simulation of the protein was performed to select relatively stable conformations for ensemble docking studies. Analyses of the RMSD plot and radius of gyration showed that the protein stabilized from 50 to 400 ns (Figure S1, Supporting Information). For the clustering process, the molecular dynamics trajectory was used as an input file; in the dimensionality reduction stage, the PCA method (principal component analysis) and *K*-means were used for the clustering method. Five structural clusters were generated from these analyses, with a silhouette score of 0.008 (Figure S2A, Supporting Information) and clusters with different dimensionalities (Figure S2B, Supporting Information). Finally, the representative conformation of each cluster was used to generate the final conformational set for MYC.

Ensemble Docking and Virtual Screening. For induced coupling studies, the AutoDock Vina 1.2.0 program was used. The five representative structures of the molecular target, generated by the EnGens tool, were analyzed on the server to identify possible binding sites. The results for predicting each conformation can be seen in Table S1, Supporting Information.

For the structure arising from cluster 0, the binding site with the highest druggability score was identified, which involved the amino acids Gly982, Arg919, Leu943, Lys936, Gly983, Ala946, Gln912, Ile942, Lys918, Thr947, Arg925, Leu931, Val940, Leu924, Ser920, Cys984, Ala937, Phe921, Val941, Lys939, Lys944, Leu917, Glu916, Pro938, Phe922, Asn915, Asn934, Gln980, and Glu935 (Table S1, Supporting Information). Docking simulations of 821 ligands against five conformations of MYC resulted in 41,050 final complexes, which were subsequently ranked according to their interaction energy values. In addition, the interaction energy value of the commercial inhibitor 1074-G5 (−8.3 kcal mol^{-1}) was used as a positive control. From the overall results, 10% (82) of the complexes with interaction energy equal to or better than that of the inhibitor were selected (Table S2, Supporting Information). In general, the interaction energy values for these 82 complexes ranged between −8.3 and −10.1 kcal mol^{-1}, and 15 complexes had an energy of −8.5 kcal mol^{-1}, 12 with −8.4 kcal mol^{-1}, and 33 with −8.3 kcal mol^{-1}.

Druglikeness and ADMET Screening. Predicting physicochemical properties and pharmacokinetic parameters *in silico* becomes a fundamental step in developing new active principles.[59] For these analyses, the stereochemistry reported in the literature was taken into account. The results for evaluating druglikeness and pharmacokinetic properties for the 82 selected ligands can be seen in Tables S3 and S4 (Supporting Information).

Solubility is a property that influences the oral bioavailability of drugs, playing a crucial role in their dissolution in the gastrointestinal environment.[60] This process represents a determining phase in gastric absorption that precedes the release of the drug into the systemic circulation.[61] Once present in the body, a substance can be subjected to several metabolization processes where toxic metabolites can be generated. The cytochrome P450 enzymes, present in the liver, for example, are responsible for around 90% of the oxidation of several drugs, and therefore, it is important to predict interactions with their isoforms.[62] The P-glycoprotein (P-gp) influences the ADMET properties of medicines and toxins; these pumps act as transporters of various compounds out of the cell with energy from ATP. The nonspecificity of substrates of these proteins can reduce the effectiveness of bioactive molecules.[63] The hERG channel blocking substances, Kv11.1, can cause prolongation of the QT interval, which is associated with the development of cardiotoxicity and an increased risk of cardiac arrest.[64] Furthermore, in the context of drug discovery, hepatotoxicity is often cited as the main reason for termination of development programs.[65]

Another important aspect in creating new drug prototypes targeted at the central nervous system is the ability of these molecules to overcome the blood−brain membrane. This natural barrier protects the central nervous system and has complicated therapy for brain disorders as most medications have difficulty reaching the brain, resulting in limited

https://doi.org/10.1021/acsomega.4c10201
ACS Omega 2024, 9, 50844−50858

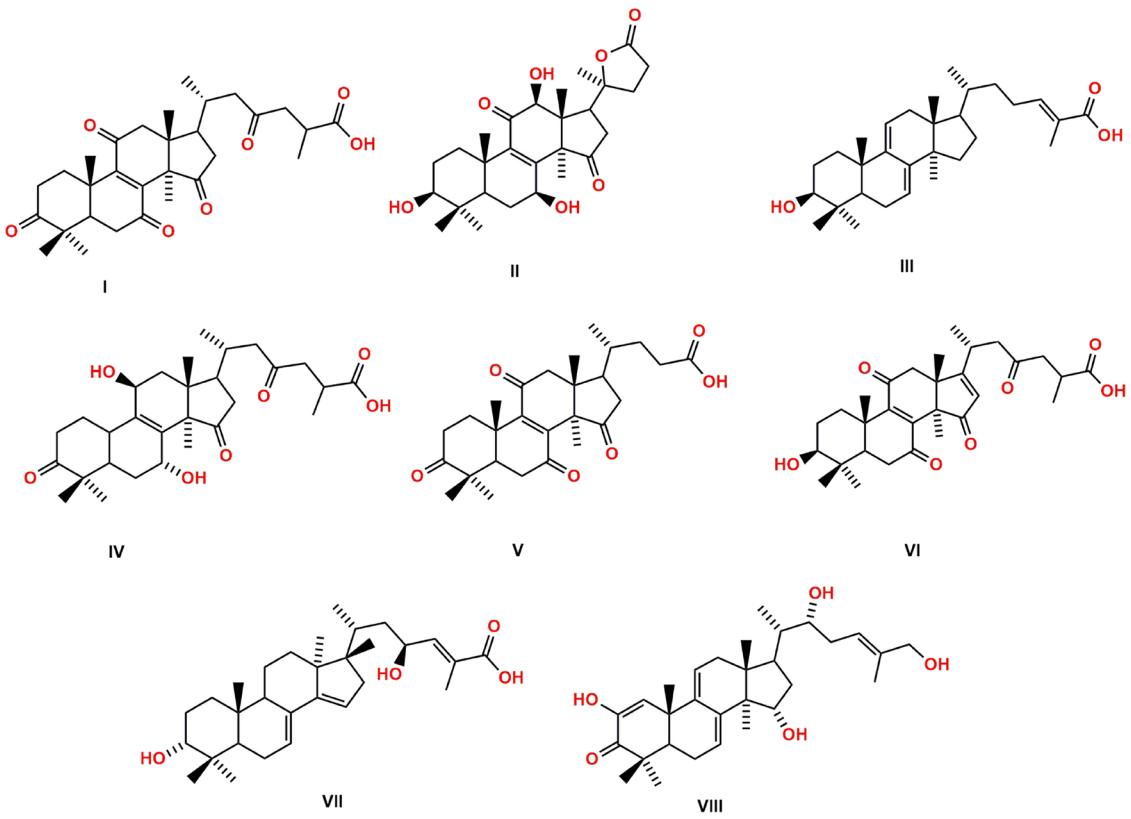

Figure 3. Chemical structures of the lanostane-type triterpene ligands 8-ene-C287 (**I**), 8-ene-C314 (**II**), 7,9-diene-C20 (**III**), 8-ene-C72 (**IV**), 8-ene-C58 (**V**), 8,16-diene-C6 (**VI**), 7,14-diene-C1 (**VII**), and 1,7,9-triene-C4 (**VIII**).

Table 1. Physicochemical Properties for Ligands I–VIII[a]

ligand	MW (Da)	cLog *P*	HBA	HBD	TPSA (Å^2)	RB	Log *S*	Log $D_{7.4}$
I	512.643	4.548	7	1	122.65	6	−5.20	1.30
II	474.594	2.482	7	3	121.13	1	−4.43	2.35
III	454.695	7.320	3	2	57.53	5	−6.16	2.09
IV	502.648	3.741	7	3	128.97	6	−4.97	1.37
V	456.579	4.343	6	1	105.58	4	−5.11	1.42
VI	512.643	4.260	7	2	125.81	6	−5.05	1.44
VII	470.694	6.291	4	3	77.76	5	−5.88	2.04
VIII	484.677	5.039	5	4	97.99	5	−5.56	2.11

[a]Notation: molecular weight (MW), partition coefficient (cLog *P*), hydrogen bond acceptors (HBA), hydrogen bond donors (HBD), topological polar surface area (TPSA), number of rotatable bonds (RB), solubility (Log *S*), and distribution coefficient (Log $D_{7.4}$).

Table 2. Pharmacokinetic Parameters for the Ligands I–VIII[a]

ligand	Pgpi (%)	Pgps (%)	HIA (%)	F30 (%)	BBB (%)	$T_{1/2}$ (h)	CL (h)	hERG (%)	H-HT (%)
I	27.00	3.70	76.30	34.60	95.30	1.72	1.45	37.80	17.40
II	58.80	2.80	70.00	45.00	93.90	1.54	1.87	36.50	43.00
III	84.10	8.70	80.8	40.90	65.90	1.96	1.16	44.20	48.40
IV	38.70	17.50	71.60	46.00	86.00	1.62	1.75	34.50	46.00
V	40.90	4.00	74.70	33.30	93.30	1.67	1.57	36.90	29.80
VI	41.20	7.00	71.60	31.80	89.80	1.74	1.64	34.70	43.60
VII	71.60	11.40	71.70	40.50	35.60	1.94	1.27	38.90	44.60
VIII	47.50	34.50	78.90	39.20	22.90	1.69	1.61	38.00	35.80

[a]Notation: P-glycoprotein inhibitor (Pgpi), P-glycoprotein substrate (Pgps), gastrointestinal absorption (HIA), bioavailability (F30), probability of crossing the blood-brain barrier (BBB), half lifetime ($T_{1/2}$), clearance rate (CL), human ether-a-go-go-related gene channel blocker (hERG), and human hepatotoxicity (H-HT).

therapeutic efficacy and potential side effects on other organs.[66] Furthermore, compounds of the same class have been effective in the treatment of brain tumors,[67−71] demonstrating the ability to cross the BBB. Thus, consider that assessing the ability to cross the BBB (>50%) is a fundamental step toward expanding the therapeutic potential

https://doi.org/10.1021/acsomega.4c10201
ACS Omega 2024, 9, 50844−50858

of ligands, allowing a broader impact in different areas of oncology.

Considering the above aspects, for the selection of the lanostane-type triterpene ligands, the following filter was used: the compound must follow Lipinski and Veber's rules and present good solubility (Log $D_{7.4}$ > 1 < 3), as well as a low probability of being a substrate for P-glycoprotein, GI-A > 50%, BBB > 50%, $T_{1/2}$ > 0.5 h, hERG < 50%, and H-HT < 50%. From these analyses, only eight ligands (Figure 3) were selected: 8-ene-C287 (**I**), 8-ene-C314 (**II**), 7,9-diene-C20 (**III**), 8-ene-C72 (**IV**), 8-ene-C58 (**V**), 8,16-diene-C6 (**VI**), 7,14-diene-C1 (**VII**), and 1,7,9-triene -C4 (**VIII**). The physicochemical properties and pharmacokinetic parameters for the eight ligands, selected based on the filter used, can be seen in Tables 1 and 2, respectively.

The selected ligands were triterpenes with carbonyl, hydroxyl, and carboxyl functional groups, that is, highly oxygenated molecules with a strong propensity to act as hydrogen bond donors or acceptors. Most of these triterpenes have acidic groups in their side chains and are related to structural similarities with the presence of unsaturation in their main skeleton. The molecular weight of these ligands varied between 442 and 512 Daltons, presenting a greater lipophilic character, a moderate surface area for the more oxygenated compounds, at least one axis of rotation, and a short but flexible side chain.

Ligand **I**, known as ganoderic acid E, was first isolated from the fungus *Ganoderma lucidum* (*G. lucidum*).[72] Ligands **II**, **III**, **IV**, and **V**, named ganoderlactone D, ganoderic acid Y, ganoderic acid Df, and lucidenic acid F, respectively, were also isolated from *G. lucidum*. Ligand **II** has already been investigated regarding its potential as an acetylcholinesterase inhibitor.[73] At the same time, ligand **III** exhibited moderate inhibition of AChE with an IC_{50} of 21.1 ± 2.66 mM,[74] antiviral activity (20 $\mu g\ mL^{-1}$),[75] the ability to inhibit the enzyme HMG-CoA (IC_{50} = 8.60 μM), and cytotoxicity against the K562 lineage (chronic myeloid leukemia) with an IC_{50} of 17.5 μM.[76] Ligand **IV** showed potent human aldose reductase inhibitory activity with an IC_{50} of 22.8 μM.[77] According to the authors of this latter study, the presence of the carboxyl group is important for activity, as its methyl ester has been shown to be much less active. Ligand **V**[78] showed potent inhibitory effects on EBV-EA induction, with IC_{50} values of 352 mol/32 pmol TPA ratio.[79] Ligand **VI**, known as ganoderic acid XL_4, was isolated from *Ganoderma theaecolum*,[80] while ligand **VII** (mariesiic acid A) was isolated from the seeds of *Abies mariesii*, a common plant in Japan.[81] Ligand **VIII**, known as phellinol E, was isolated from the fungus *Phellinus igniarius* and showed cardioprotective activity against oxygen-glucose deprivation/reoxygenation injury in H9c2 cells at a concentration of 20 μM.[82]

Analyses of the Complex Interactions. The complexes formed with the eight ligands selected in the screening of the druglikeness and physicochemical parameters were analyzed to understand the molecular behavior of these triterpenes at the MYC site. Table 3 shows the ligands that interacted most effectively with the protein, highlighting the amino acid residues involved in the interactions, the number of hydrogen bonds, bond distance, and the value of the interaction energy of the complexes. Thus, we expect that these ligands may inhibit the formation of the MYC-MAX complex. This type of inhibition may occur through conformational changes in MYC, limiting the binding interface with MAX. Furthermore, these ligands may compete with MAX for shared binding regions on MYC, decreasing the availability of MYC to form the MYC-MAX complex. Small molecules (NSC13728, PKUMDL-YC-1101, PKUMDL-YC-1201, PKUMDL-YC-1202, PKUMDL-YC-1203, PKUMDL-YC-1204, PKUMDL-YC-1301, and L755507)[37,38,40] identified from computational studies were able to interact with the bHLH-LZ domain of MYC and destabilize the formation of the MYC-MAX complex and reduce its oncogenic activity.[37,38,40]

Table 3. Molecular Docking Results for Complexes MYC-I–MYC-VIII

ligand code	energy (kcal mol^{-1})	H bond	amino acids	distance (Å)
I	−8.6	3	Arg919, Ser920, and Phe921	2.69, 2.12, 1.80
II	−8.5	3	Leu917, Arg919, and Ser920	1.91, 2.76, 2.92
III	−8.4	3	Arg919, Ser920, and Phe921	2.03, 2.21, 2.02
IV	−8.3	3	Arg919, Ser920, and Phe921	2.33, 2.16, 1.93
V	−8.3	3	Arg919, Ser920, and Phe921	2.09, 2.29, 2.29
VI	−8.3	3	Arg919, Ser920, and Phe921	2.33, 2.22, 2.29
VII	−8.3	3	Arg919, Ser920, and Phe921	2.10, 2.17, 2.13
VIII	−8.3	2	Ser920 and Glu935	2.88, 2.71

The ligands **I**, **III**, **IV**, **V**, **V**, **VI**, and **VII**, due to their structural similarities, formed complexes with MYC through hydrogen bonds involving the amino acids Glu916, Arg919, Ser920, and Phe921 with carboxylate groups present in their side chain (Figure 3); the interaction energy of these complexes varied between −8.3 and −8.6 kcal mol^{-1} (Table 3).

Ligand **VIII** formed a complex with an energy of −8.3 kcal mol^{-1} and made two hydrogen bonds with the amino acids Glu935 and Ser920 with the hydroxyl oxygen present in the side chain and carbonyl present in the C-3 position. Ligand **II** interacted with MYC with an energy of −8.5 kcal mol^{-1} through three hydrogen bonds involving the hydroxyl at C-12 and the carbonyl of the lactone functional group with the amino acids Leu917, Arg919, and Ser920 (Table 3 and Figure S3, Supporting Information).

Considering the absolute value of the interaction energy, the best results were for ligands **I** and **II**. Regarding the interactions involving the amino acids Leu917, Ser920, Phe921, Leu943, and Lys939, it is worth noting that these have already been previously reported for new MYC inhibitor prototypes.[39,83,84] These amino acids are in the helix–loop–helix region of MYC and are responsible for important interactions for the dimerization process with the MAX protein. When ligands bind to these amino acids, they can interfere with the interaction with the MAX protein, which can impair the formation of the MYC-MAX complex.[39,83,84] In addition, comparing the interaction energy values of the complexes generated in this study with energy values of complexes formed with ligands described in the literature (D347-2761, 7594-0037, L755507, and 10074-65, Table S2, Supporting Information) and designed for inhibition of MYC or MYC-MAX, we verified a better molecular complementarity in our results (Table S2, Supporting Information).

https://doi.org/10.1021/acsomega.4c10201
ACS Omega 2024, 9, 50844−50858

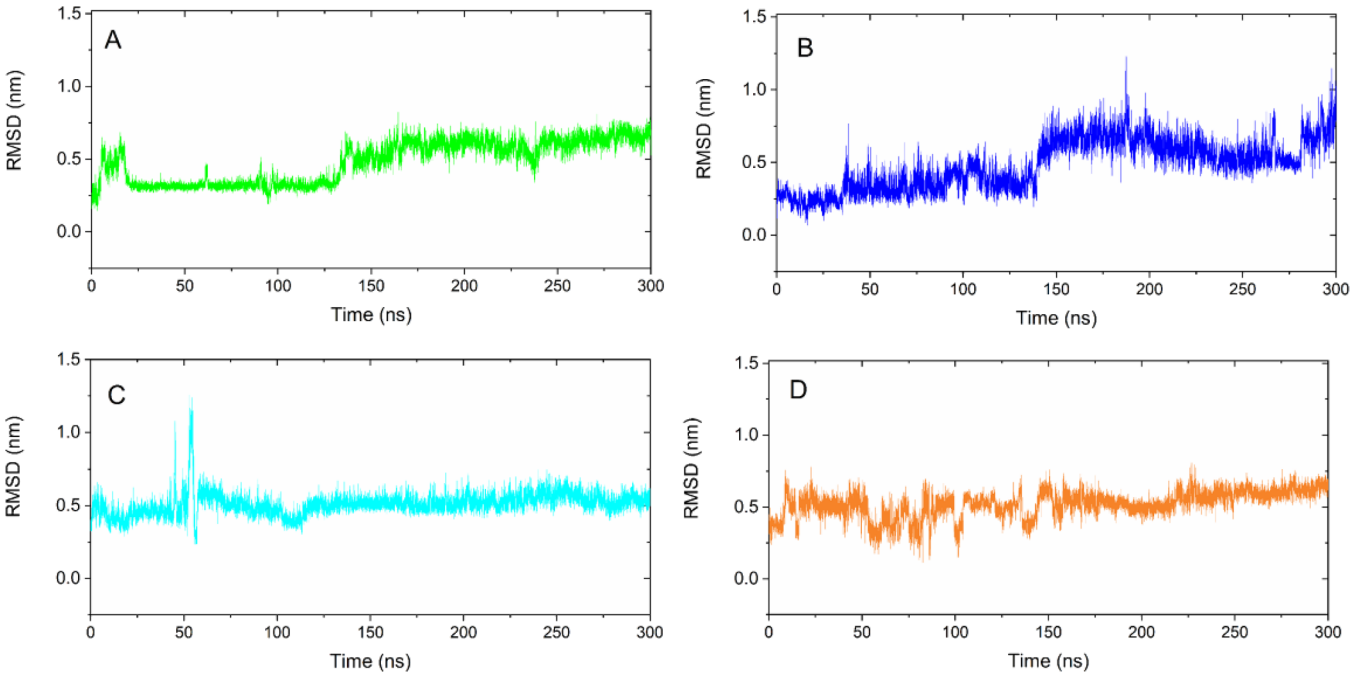

Figure 4. RMSD graph for the complexes. (A) MYC-**I** (green line), (B) MYC-**IV** (blue line), (C) MYC-**VI** (cyan line), and (D) MYC-**VII** (orange line).

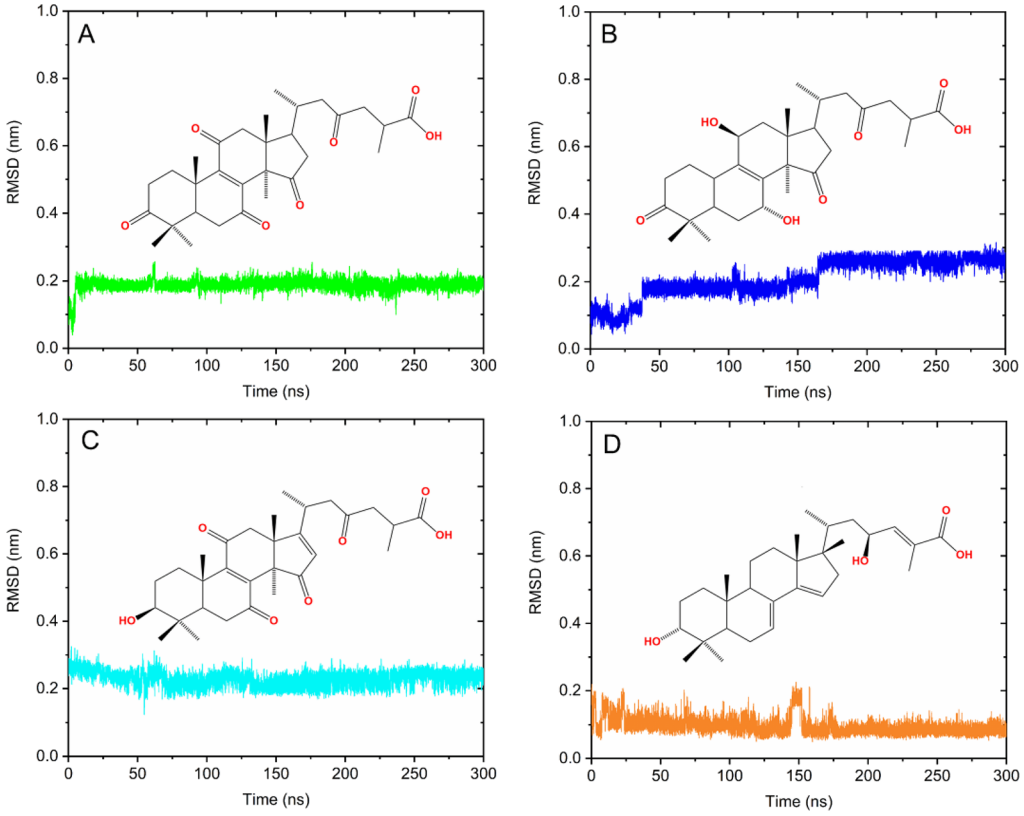

Figure 5. RMSD plot for ligands. (A) Ligand **I** (green line), (B) ligand **IV** (blue line), (C) ligand **VI** (cyan line), and (D) ligand **VII** (orange line).

Molecular Dynamics Analysis. MD simulations of 300 ns were performed to discern the stability of the best results obtained in the molecular docking study. To analyze the physical movement and to predict conformational changes at the molecular level, calculations of root-mean-square deviation (RMSD), root-mean-square fluctuation (RMSF), radius of gyration (Rdg), and hydrogen bonds for the complexes (MYC-**I**−MYC-**VIII**) were analyzed.

Analysis of the RMSD of the Complexes. The RMSD in molecular dynamics simulations is a measure that evaluates the variability of atomic positions relative to a reference structure.[85] The RMSD evaluation identifies whether the

https://doi.org/10.1021/acsomega.4c10201
ACS Omega 2024, 9, 50844−50858

complex is maintaining its conformational integrity or whether there are significant changes over the simulation time. High RMSD values are associated with more severe conformational changes, while lower values indicate low structural mobility. As observed in the RMSD analysis (Figure S4, Supporting Information), some complexes reached equilibrium at the beginning of the simulation (**I**, **VI**, and **VII**), while others exhibited some fluctuations before equilibrium (**V** and **VIII**) or took most of the simulation to stabilize (**II** and **III**). Overall, RMSD values spanned from 0.48 to 1.34 nm, which reveals relatively low mobility for these systems[86] (Figure S4, Supporting Information). The complexes formed with ligands **I**, **IV**, **VI**, and **VII** showed greater stability in relation to RMSD values, and their trajectories were analyzed in more detail. The MYC-**I** complex showed stability between 21 and 130 ns, then suffered small fluctuations, and stabilized again from 135 ns until the end of the simulation, with an average RMSD of 0.48 nm (Figure 4, green line). The MYC-**IV** complexes (Figure 4, blue line) showed two stability levels from 40 to 139 ns and 142 to 300 ns; the average RMSD value was 0.48 nm. Analyzing the MYC-**VI** complex (Figure 4, cyan line), we can see a greater stability range that starts from 60 ns and remains practically constant until the end of the simulation; the average RMSD value was 0.51 nm (Figure 4, cyan line). The MYC-**VII** complex showed slight fluctuations in RMSD during the initial 150 ns. It reached relative stability between 160 and 300 ns, with the average RMSD value being 0.52 nm (Figure 4, orange line). For these complexes, it is reinforced that the main conformational changes in the structure of MYC occur mainly in its side chains. The RMSD results for these complexes were promising, as they presented significantly low values with little difference between them. However, considering the absolute mean RMSD value for these complexes, ligands **I**, **IV**, and **VI** were able to interact more effectively with MYC as they showed lower RMSD values. Comparing the results shown in the RMSD graphs of the complexes obtained in this study (Figure 4) with those described,[40,83] we can verify that the triterpenes used in this study were able to stabilize the MYC structure more quickly and that the average RMSD value was significantly lower, therefore generating more stable complexes. Such behavior may influence the inhibitory potential for these ligands, but to date, a direct relationship between RMSD variation and pharmacological action for this target has not been reported.

RMSD Analysis for the Ligands at the MYC Binding Site. The molecular behavior of ligands 8-ene-C287 (**I**), 8-ene-C72 (**IV**), 8,16-diene-C6 (**VI**), and 7,14-diene-C1 (**VII**), while interacting with residues at the MYC binding site, was analyzed. The RMSD plot of ligands along 300 ns of simulation is shown in Figure 5. Ligands **IV** and **VI** presented plateaus with RMSD variations and an average value of 0.20 and 0.22 nm, respectively. On the other hand, ligands **I** and **VII** showed a greater stability range throughout the simulation with RMSD values of 0.18 and 0.09 nm, respectively. These results show that the ligands underwent few changes in their conformations when bonded to MYC, reflecting their stabilization at the binding site.

RMSF Analysis for the Complexes. RMSF was used to investigate the flexibility of specific residues of the complexes over time. Discrete fluctuations indicate greater relative stability for the complex. On the other hand, more pronounced fluctuations indicate less stabilization.[87] The graphs relating to these analyses are shown in Figure 6. More specifically, in the

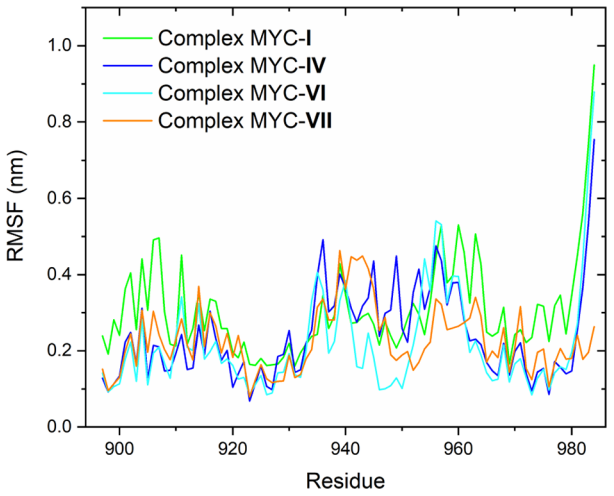

Figure 6. RMSF plot for the complexes MYC-**I** (green line), MYC-**IV** (blue line), MYC-**VI** (cyan line), MYC-**VII** (orange line), and native MYC (black line).

MYC-**IV**, MYC-**VI**, and MYC-**VII** complexes, slight fluctuations were observed in amino acids in regions 906−924 and 965−980, which reflect greater flexibility. Amino acids between 930 and 960, in the central region of the protein, showed more pronounced fluctuations for all complexes (Figure 6). Only the MYC-**I** and MYC-**IV** complexes showed high flexibility when considering the final region. These results show that the presence of the ligands assists in protein stabilization.

Analysis of the Radius of Gyration of the Complexes. The radius of gyration (Rdg) was used to evaluate the complexes' size, compactness, and conformational changes throughout the MD simulation. In general, low Rdg values indicate more stable and compact conformations, while higher values are associated with less compact and more expanded structures.[88] In addition, compaction indicates how molecules are organized and whether they are in conformations that favor effective interactions.[89] More compact complexes tend to have a configuration that facilitates interaction between components and are therefore more stable, as the interaction between molecules is stronger.[90] Rdg results are depicted in Figure 7. The complexes MYC-**I**, MYC-**IV**, MYC-**VI**, and MYC-**VII** generally exhibited similar behavior, showing few variations along the trajectory, with values below 1.5 nm.

This shows that, despite the conformational changes in the structure of the MYC protein and ligands throughout the simulation run, the compactness remained practically unchanged.

Analysis of Hydrogen Bonds during MD. Evaluating the ability of new prototype inhibitors to form hydrogen bonds with specific molecular targets has been a useful strategy for drug screening and design.[91] The graphs illustrated in Figure S5 (Supporting Information) show that the ligands established interactions with the MYC protein, promoting the formation of hydrogen bonds that help stabilize the complexes. By analyzing the graphs (Figure S5, Supporting Information), ligands **I** and **VII** showed greater oscillations in the number of hydrogen bonds throughout the simulation; for ligand **I**, the number of bonds was between 1 and 4 and for ligand **VII** between 1 and 7 bonds. On the other hand, ligands **IV** and **VI** showed smaller variations in the number of bonds, for ligand **IV** from 4 to 6 bonds on average, and for ligand **VI** between 2 and 4 bonds on average. Thus, the ability of the ligands to carry out stable

https://doi.org/10.1021/acsomega.4c10201
ACS Omega 2024, 9, 50844−50858

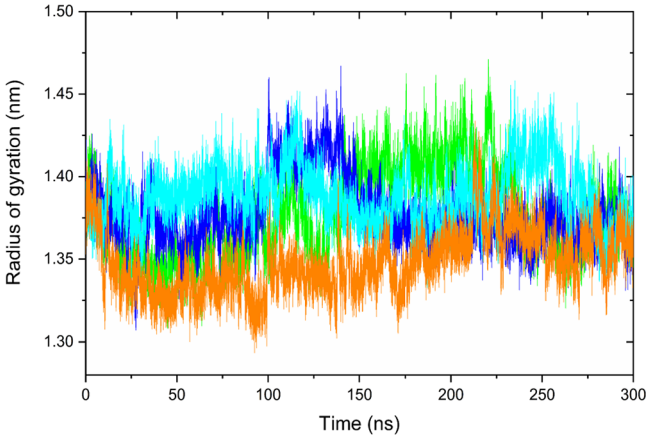

Figure 7. Radius of gyration graph for complexes MYC-**I** (green line), MYC-**IV** (blue line), MYC-**VI** (cyan line), and MYC-**VII** (orange line).

interactions through hydrogen bonds reinforces the conclusions observed in the RMSD and RMSF, and the radius of gyration analyzes and supports the possibility of these ligands having an anticancer therapeutic effect via inhibition of the MYC protein.

Analysis of Complex Interactions during MD. The integrity of the MYC-**I**, MYC-**IV**, MYC-**VI**, and MYC-**VII** complexes during the 300 ns MD trajectories was verified through analysis in the VMD 1.9.4a51 program.[92] In general, the ligands remained associated with the MYC binding site, only modifying the types of interactions with the amino acids. Figure 8 shows a summary of the conformations adopted

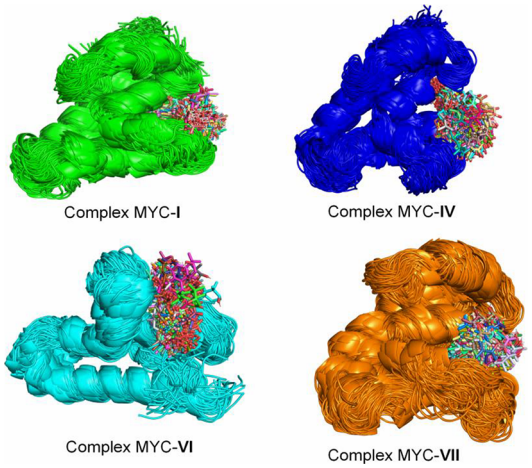

Figure 8. Conformational ensemble of the complexes MYC-**I**, MYC-**IV**, MYC-**VI**, and MYC-**VII** during the 300 ns trajectory.

during the simulations for each complex. The ligands investigated formed multiple bonds (hydrophobic and hydrophilic) with the molecular target during the trajectory. These interactions involved the amino acids Leu917, Arg919, Ser920, Phe921, Leu943, Val940, Lys939, Glu916, Ile942, Ala937, Tyr949, Arg925, Pro938, and Leu93, between others (Figures S6–S9, Supporting Information).

Binding Energy Calculation Analysis Using the MM-GBSA Method. The MM-GBSA technique is often used to calculate protein–ligand complexes' final state binding energy.[93] For the analysis of this study, the last 10 ns (100 frames) of relatively stable trajectories (290–300 ns) was analyzed, at a temperature of 303.15 K. The influence of the external dielectric constant of the solvent on the calculation of binding energy was investigated for values 20, 40, and 80. The binding energy value did not show significant changes for the analyzed constant values (Figure S10, Supporting Information). However, a slightly different response was obtained for the internal solute dielectric constant of 2 and the external solute dielectric constant of 20. The contributions of the energetic terms associated with the (ΔE_{Bind}) binding energy calculation for the MYC-**I**, MYC-**IV**, MYC-**VI**, and MYC-**VII** complexes are shown in Figure 9. The binding energy

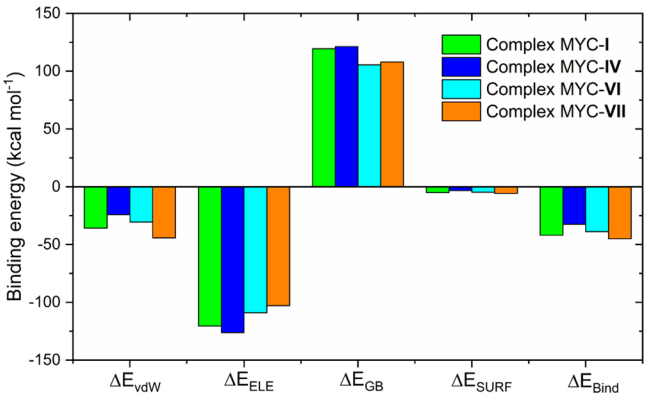

Figure 9. Contributions of the energetic terms associated with the binding energy calculation for the MYC-**I**, MYC-**IV**, MYC-**VI**, and MYC-**VII** complexes.

decomposition analysis showed positive values for polar solvation energy (ΔE_{GB}) and negative values for van der Waals interaction energy (ΔE_{vdW}), electrostatic (ΔE_{ELE}), and nonpolar contributions (ΔE_{SURF}). The electrostatic interaction energy values were more significant than the van der Waals interaction energy for final energy (Figure 9). This behavior can be justified by the presence of functional groups (carboxylate) charged on the side chain of the ligands. For the MYC-**I**, MYC-**IV**, MYC-**VI**, and MYC-**VII** complexes, energies of -41.96 ± 3.03, -32.48 ± 3.41, -38.83 ± 2.59, and -44.98 ± 4.41 kcal mol^{-1} were found, respectively (Figure 9). These results are in agreement with the binding energy described for MYC complexes in previous studies.[40,75] Binding energy values reflect the magnitude of interactions between ligands and proteins, making it possible to estimate the relative stability of these dynamic systems.[94] In this case, the interactions of the molecular target MYC with the ligands 7,14-diene-C1 (**VII**) proved to be energetically more favorable compared to the other ligands. Such observations suggest strong connections in the complexes, which can be translated as greater inhibitory action and, consequently, greater potential for therapeutic effects.

The contribution of the main amino acid residues to the energy of binding was investigated, covering amino acids distant up to 10 Å from the ligands (Figure 10). The most favorable contributions were identified in the four complexes (MYC-**I**, MYC-**IV**, MYC-**VI**, and MYC-**VII**), and the complexes exhibited distinct energetic decompositions for the binding energy. In the MYC-**I** complex, the main contributions were Phe921 (ΔE = −3.66 kcal mol^{-1}), Lys939 (ΔE = −2.05 kcal mol^{-1}), Ile942 (ΔE = −2.53 kcal mol^{-1}), and Leu943 (ΔE = −2.29 kcal mol^{-1}) (Figure 10). In

https://doi.org/10.1021/acsomega.4c10201
ACS Omega 2024, 9, 50844−50858

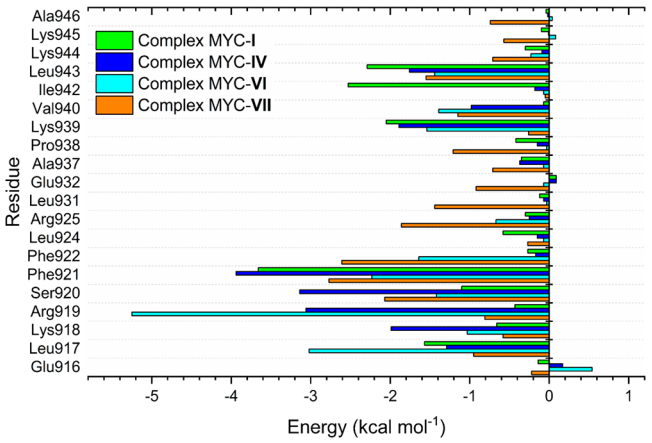

Figure 10. Contributions of the energetic terms associated with the binding energy calculation for the MYC-**I**, MYC-**IV**, MYC-**VI**, and MYC-**VII** complexes.

the MYC-**IV** complex, the main contributions were Arg919 (ΔE = −3.06 kcal mol^{-1}), Ser920 (ΔE = −3.14 kcal mol^{-1}), and Phe921 (ΔE = −3.94 kcal mol^{-1}) (Figure 10). For the MYC-**VI** complex, the contributions of amino acid residues Leu917 (ΔE = −3.02 kcal mol^{-1}), Arg919 (ΔE = −5.25 kcal mol^{-1}), and Phe921 (ΔE = −2.18 kcal mol^{-11}) (Figure 10) were obtained. Completion analysis of the MYC-**VII** complex showed that amino acids developed more for binding energy binding of Ser920 (ΔE = −2.07 kcal mol^{-1}), Phe921 (ΔE = −2.77 kcal mol^{-1}), and Phe922 (ΔE = −2.61 kcal mol^{-1}) (Figure 10). The amino acids Leu917, Ser920, and Phe921 showed strong contributions to binding energy in previous studies, and as hot spots, the amino acids Leu924, Gln927, and Leu943 stood out.[40]

Based on the computational studies carried out so far, the 7,14-diene-C1 (**VII**) ligand stands out as the hit compound for MYC inhibition. This triterpene showed an interaction energy of −8.3 kcal mol^{-1}, follows those of Lipinski and Veber, has ADMET parameters within the filter used, and showed strong interaction with a molecular target in molecular dynamics simulation studies, justified through RMSD, RMSF, Rdg, and hydrogen bonds analyses. The complex formed with this triterpene showed the best binding energy with a value of −42.64 kcal mol^{-1}. A triterpene belonging to the class of compounds called pisosterol has shown anticancer potential[54−56,95] and the ability to act in the attenuation of cancer cell lines with MYC overexpression.[57,58] Therefore, all these results are important and could represent a breakthrough for developing new agents of anticancer and MYC inhibitors.

METHODS

Ligand Library and Preparation. The lanostane-type triterpene compounds were selected from articles published in the literature between 1956 and 2022. The 2D structures of the compounds (ligands) were generated using ChemDraw Ultra 12.0 software.[96] Avogadro software (version 1.2) was employed to produce 3D conformations and to perform energy minimization procedures using the universal force field (UFF).[97] When necessary, Open Babel (version 2.3.1) was employed to convert 3D structures into pdbqt format.[98] The (*R*) or (*S*) stereochemistry of each lanostane-type triterpene structure was represented as indicated in the original literature.

Molecular Target Selection and Preparation. The three-dimensional structure of the MYC-MAX heterodimer complexed to the DNA molecule was obtained from the Protein Data Bank (PDB)[99] with the ID 1NKP.[100] In PyMOL v2.5.3 software,[101] MYC was separated from the MAX protein and DNA molecule, and the water molecules were removed. The protonation step at pH 7.4 was performed using the PROPKA algorithm, available on the PDB2PQR server (https://server.poissonboltzmann.org/pdb2pqr),[102] and the stereochemical quality of the protein was evaluated by the Ramachandran plot generated from the PROCHECK server (https://saves.mbi.ucla.edu/).[103]

Conformational Ensemble. Initially, using the GROMACS v2023 program,[104] a 400 ns MD simulation of the protein in water was carried out to obtain relatively stable conformations during the trajectory. To carry out the simulation, the traditional protocol was used, which consists of the steps of preparing the topology files, defining the box and solvent, adding ions, minimizing energy, equilibration, and production. From the MD trajectory, the EnGens tool was used to build the representative conformational set of the molecular target, according to the methodology described by Conev and co-workers (https://github.com/KavrakiLab/EnGens).[105]

Determination of the Binding Site. The CavityPlus web server was used to evaluate possible binding sites in the protein's three-dimensional structure (http://www.pkumdl.cn:8000/cavityplus/index.php).[106] This tool identifies pockets in three-dimensional protein structures and classifies them with drug scores and druggability scores. The search for binding sites was carried out using the five conformations generated by the EnGens tool. The binding site was selected based on the druggability score and similarity with previous studies.[40,84]

Ensemble Docking. Molecular docking simulations were performed using AutoDock Vina 1.2.0.[107] Five three-dimensional structures of the molecular target generated by the EnGens tool were used, with a simulation box centered at 58.75, 63.75, and 52.50 for the *X*, *Y*, and *Z* coordinates, respectively, and a size of 15 × 12 × 14 Å.

Druglikeness Prediction and Pharmacokinetic Parameters. The SwissADME webserver (http://www.swissadme.ch/)[108] was used to estimate the druglikeness, distribution coefficient (Log $D_{7.4}$), and aqueous solubility (Log *S*) of the ligands. In addition, the Lipinski and Veber rules were used for screening through oral bioavailability.[109,110] To evaluate these rules, the molecular weight (MW), number of hydrogen bond donor (HBD) and acceptor (HBA) atoms, partition coefficient (cLog *P*), topological polar surface area (TPSA), and number of rotatable bonds (RB) were analyzed. The evaluation of the absorption, distribution, metabolism, elimination, and toxicity (ADMET) parameters of the lanostane-type triterpenes was carried out using the ADMETlab platform (https://admet.scbdd.com/home/index/).[111] The properties analyzed for screening were the P-glycoprotein inhibitor (Pgpi), P-glycoprotein substrate (Pgps), gastrointestinal absorption (HIA), bioavailability (F30), probability of crossing the blood−brain barrier (BBB), half lifetime ($T_{1/2}$), clearance rate (CL), human ether-a-go-go-related gene (hERG) channel blocker, and human hepatotoxicity (H-HT).

Molecular Dynamics Simulations. Molecular dynamics (MD) simulations were conducted using GROMACS 2023 software.[104,112] For the protein under study, the topology

https://doi.org/10.1021/acsomega.4c10201
ACS Omega 2024, 9, 50844−50858

parameters were defined with the aid of the AMBER99SB force field.[113] The topology parameters for the ligands were generated using the ACPYPE (AnteChamber Python Parser interfacE) server (https://www.bio2byte.be/acpype/).[114,115] The initial conformation of the ligands used for each complex was the best pose, selected from induced coupling studies carried out using the ensemble docking technique. Each complex was solvated in a cubic box with tip3p water, with periodic boundary conditions applied, and the system neutralized with Na^+ or Cl^- ions (0.15 mol L^{-1}). Before the simulation, each complex underwent energy minimization, which consisted of 10,000 steps of the steepest descent algorithm followed by a 10,000-step conjugate gradient algorithm, thus ensuring system stability. Subsequently, each molecular model was gradually heated from 0 to 303.15 K in the isothermal isovolumetric (NVT) ensemble for 200 ps. It was then equilibrated for 1.0 ns in the isothermal−isobaric set (NPT) at 303.15 K and 1.0 atm.

Calculation of Binding Energy (MM-GBSA). The gmx_MMPBSA 1.6.3 package, an efficient GROMACS tool, was used to calculate binding energy using the MM-GBSA method (https://valdes-tresanco-ms.github.io/gmx_MMPBSA/dev/).[116] To calculate the binding energy, the last 10 ns of relative stability (100 frames) of the complex's trajectory (290−300 ns) were used, with an internal dielectric constant of 2, external dielectric constants of 20, 40, 80, and a temperature of 303.15 K. The contribution of the total energy components ΔG_{Bind} is described in eqs 1−3below, where $\Delta G_{complex}$, $\Delta G_{receptor}$, and ΔG_{ligand} represent the estimated binding energy of the complex, protein, and ligand, respectively. ΔG_n refers to the contribution of each individual entity (complex, protein, and ligand). The term ΔE_{Gas} represents the variation in interaction energy between the protein and the ligand in the gas phase, obtained through van der Waals (ΔE_{vdW}) and electrostatic (ΔE_{ELE}) interactions. Meanwhile, the term ΔE_{sol} reflects the binding energy of solvation, derived by calculating the polar (ΔE_{GB}) and nonpolar contributions. Finally, $T\Delta S$ corresponds to the entropy term but was not considered in the calculations.

$$\Delta G_{Bind} = \Delta G_{complex} - (\Delta G_{receptor} + \Delta G_{ligand}) \quad (1)$$

$$\Delta G_n = \Delta E_{Gas} + \Delta E_{sol} - T\Delta S \quad (2)$$

$$\Delta G_n = \Delta E_{vdW} + \Delta E_{ELE} + \Delta E_{GB} + \Delta E_{SURF} - T\Delta S \quad (3)$$

CONCLUSIONS

The anti-MYC potential of triterpenes was evaluated using computational approaches involving molecular docking, MD, and binding energy calculation. Using the EnGens tool, the relatively stable MYC protein conformational ensemble was generated to track the initial binding poses of the triterpenes. In the docking studies, 82 ligands were selected based on the interaction energy values between −8.3 and −10.1 kcal mol^{-1}. The virtual screening of these 82 triterpenes using physicochemical (druglikeness) and pharmacokinetic (ADMET) properties allowed the selection of eight triterpenes. The stability of these eight complexes was analyzed by 300 ns MD simulations. The RMSD, RMSF, and radius of gyration plots revealed that four ligands, 8-ene-C287 (**I**), 8-ene-C72 (**IV**), 8,16-diene-C6 (**VI**), and 7,14-diene-C1 (**VII**), effectively interacted with the protein during the simulation and helped its stabilization. The binding energy was calculated using the MM-GBSA method and presented energies between −32.48 and −44.98 kcal mol^{-1} for the complexes MYC-**I**, MYC-**IV**, MYC-**VI**, and MYC-**VII**.

The computational results obtained in this study support the hypothesis of strong interactions between the molecular target and the lanostane-type ligands, especially for the 7,14-diene-C1 (**VII**) ligand, which was considered a hit compound. This behavior may suggest a possible inhibitory action for these molecules, motivating further *in vitro* anti-MYC experiments.

ASSOCIATED CONTENT

Data Availability Statement

To construct the conformational set of the MYC protein, the EnGens pipeline provided on GitHub (https://github.com/KavrakiLab/EnGens/blob/main/README.md) was used. Ensemble docking studies were carried out using the free AutoDock Vina v1.2.0 program. MD simulations were conducted in GROMACS 2023. The energy calculation using the MM-GBSA method was performed using the gmx_MMPBGBSA 1.6.3 package available on GitHub (https://valdes-tresanco-ms.github.io/gmx_MMPBSA/dev/). The input files and main results can be located in Zenodo (10.5281/zenodo.11226836).

Supporting Information

The Supporting Information is available free of charge at https://pubs.acs.org/doi/10.1021/acsomega.4c10201.

MD for MYC protein; MD trajectory clustering of MYC protein obtained by the EnGens pipeline; molecular docking poses for the top eight complexes; RMSD plots for the top eight complexes; hydrogen bonding plots for the complexes with ligands **I**, **IV**, **VI**, and **VII**; interactions observed in MYC-**I**, MYC-**IV**, MYC-**VI**, and MYC-**VII** complexes during the 300 ns MD trajectory; influence of the solvent dielectric constant on interaction energy calculation; binding sites identified by the CavityPlus server; interaction energy results for the 82 ligands; druglikeness, physicochemical, and pharmacokinetic properties for the 82 selected ligands (PDF)

AUTHOR INFORMATION

Corresponding Authors

Geancarlo Zanatta − *Department of Biophysics, Bioscience Institute, Federal University of Rio Grande do Sul, Av. Bento Gonçalves, Porto Alegre, RS 91501-970, Brazil*; Email: geancarlo.zanatta@ufrgs.br

Maria C. F. Oliveira − *Department of Organic and Inorganic Chemistry, Science Center, Federal University of Ceará, Fortaleza, CE 60455-760, Brazil*; orcid.org/0000-0002-7445-2347; Email: mcfo@ufc.br

Authors

José A. C. Oliveira − *Department of Organic and Inorganic Chemistry, Science Center, Federal University of Ceará, Fortaleza, CE 60455-760, Brazil*

Jonatas M. Negreiro − *Department of Organic and Inorganic Chemistry, Science Center, Federal University of Ceará, Fortaleza, CE 60455-760, Brazil*; orcid.org/0000-0003-0013-1791

Fátima M. Nunes − *Department of Organic and Inorganic Chemistry, Science Center, Federal University of Ceará, Fortaleza, CE 60455-760, Brazil*

https://doi.org/10.1021/acsomega.4c10201
ACS Omega 2024, 9, 50844−50858

Francisco G. Barbosa − *Department of Organic and Inorganic Chemistry, Science Center, Federal University of Ceará, Fortaleza, CE 60455-760, Brazil*

Jair Mafezoli − *Department of Organic and Inorganic Chemistry, Science Center, Federal University of Ceará, Fortaleza, CE 60455-760, Brazil;* orcid.org/0000-0002-0148-0494

Marcos C. Mattos − *Department of Organic and Inorganic Chemistry, Science Center, Federal University of Ceará, Fortaleza, CE 60455-760, Brazil;* orcid.org/0000-0003-4291-5199

Maria C. R. Fernandes − *Drug Research and Development Center, Federal University of Ceará, Fortaleza, CE 60430-275, Brazil*

Claudia Pessoa − *Drug Research and Development Center, Federal University of Ceará, Fortaleza, CE 60430-275, Brazil*

Cristiana L. M. Furtado − *Drug Research and Development Center, Federal University of Ceará, Fortaleza, CE 60430-275, Brazil; Graduate Program in Medical Sciences, University of Fortaleza, Fortaleza, CE 60811-650, Brazil*

Complete contact information is available at: https://pubs.acs.org/10.1021/acsomega.4c10201

Funding

The Article Processing Charge for the publication of this research was funded by the Coordination for the Improvement of Higher Education Personnel - CAPES (ROR identifier: 00x0ma614).

Notes

The authors declare no competing financial interest.

■ ACKNOWLEDGMENTS

The authors thank the Coordenação de Aperfeiçoamento de Ensino Superior (CAPES) for financial support (Finance Code 001-PROEX 23038.000509/2020-82; AUXPE No. 1227/2020). J. A. C. Oliveira and J. M. Negreiro thank Conselho Nacional de Desenvolvimento Científico e Tecnológico (CNPq, Process: 160441/2021-8) and Fundação Cearense de Apoio ao Desenvolvimento Científico e Tecnológico (FUNCAP, Process: BMD-0008-01997.01.20/22) for their doctorate sponsorships. M. C. F. Oliveira (Process: 305148/2023-0), M. C. Mattos (Process: 306289/2021-0), and C. Pessoa (Process: 305509/2023-3) thank Conselho Nacional de Desenvolvimento Científico e Tecnológico (CNPq) for their research grant. The authors are also thankful to the Centro Nacional de Processamento de Alto Desempenho from UFC (CENAPAD/UFC) and the Centro Nacional de Supercomputação from UFRGS (CESUP/UFRGS) for the computer cluster facilities.

■ REFERENCES

(1) Dalla-Favera, R.; Bregni, M.; Erikson, J.; Patterson, D.; Gallo, R. C.; Croce, C. M. Human C-Myc Onc Gene Is Located on the Region of Chromosome 8 That Is Translocated in Burkitt Lymphoma Cells. *Proc. Natl. Acad. Sci. U. S. A.* **1982**, *79* (24), 7824−7827.

(2) Henriksson, M.; Luscher, B. Proteins of the Myc Network: Essential Regulators of Cell Growth and Differentiation. *Adv. Cancer Res.* **1996**, *68*, 109−182.

(3) Dang, C. V.; Resar, L. M. S.; Emison, E.; Kim, S.; Li, Q.; Prescott, J. E.; Wonsey, D.; Zeller, K. Function of the C-Myc Oncogenic Transcription Factor. *Exp. Cell Res.* **1999**, *253* (1), 63−77.

(4) Dang, C. V.; O'Donnell, K. A.; Zeller, K. I.; Nguyen, T.; Osthus, R. C.; Li, F. The C-Myc Target Gene Network. *Semin. Cancer Biol.* **2006**, *16* (4), 253−264.

(5) Jha, R. K.; Kouzine, F.; Levens, D. MYC function and regulation in physiological perspective. *Front. Cell Dev. Biol.* **2023**, *11*, No. 1268275.

(6) Kalkat, M.; De Melo, J.; Hickman, K. A.; Lourenco, C.; Redel, C.; Resetca, D.; Tamachi, A.; Tu, W. B.; Penn, L. Z. MYC Deregulation in Primary Human Cancers. *Genes (Basel).* **2017**, *8* (6), 151.

(7) Sorolla, A.; Wang, E.; Golden, E.; Duffy, C.; Henriques, S. T.; Redfern, A. D.; Blancafort, P. Precision Medicine by Designer Interference Peptides: Applications in Oncology and Molecular Therapeutics. *Oncogene* **2020**, *39* (6), 1167−1184.

(8) Trop-Steinberg, S.; Azar, Y. Is Myc an Important Biomarker? Myc Expression in Immune Disorders and Cancer. *Am. J. Med. Sci.* **2018**, *355* (1), 67−75.

(9) Dhanasekaran, R.; Deutzmann, A.; Mahauad-Fernandez, W. D.; Hansen, A. S.; Gouw, A. M.; Felsher, D. W. The MYC Oncogene - the Grand Orchestrator of Cancer Growth and Immune Evasion. *Nat. Rev. Clin. Oncol.* **2022**, *19* (1), 23−36.

(10) Burrell, R. A.; McGranahan, N.; Bartek, J.; Swanton, C. The causes and consequences of genetic heterogeneity in cancer evolution. *Nature* **2013**, *501*, 338−345.

(11) Bahram, F.; von der Lehr, N.; Cetinkaya, C.; Larsson, L. G. c-Myc hot spot mutations in lymphomas result in inefficient ubiquitination and decreased proteasome-mediated turnover. *Blood* **2000**, *95*, 2104−2110.

(12) Sur, I.; Taipale, J. The role of enhancers in cancer. *Nat. Rev. Cancer* **2016**, *16*, 483−493.

(13) Fatma, H.; Maurya, S. K.; Siddique, H. R. Epigenetic modifications of c-MYC: Role in cancer cell reprogramming, progression and chemoresistance. *Semin. Cancer Biol.* **2022**, *83*, 166−176.

(14) Lee, J. M.; Hammarén, H. M.; Savitski, M. M.; Baek, S. H. Control of protein stability by post-translational modifications. *Nat. Commun.* **2023**, *14*, 201.

(15) Schaub, F. X.; Dhankani, V.; Berger, A. C.; Trivedi, M.; Richardson, A. B.; Shaw, R.; Zhao, W.; Zhang, X.; Ventura, A.; Liu, Y.; Ayer, D. E.; Hurlin, P. J.; Cherniack, A. D.; Eisenman, R. N.; Bernard, B.; Grandori, C.; Caesar-Johnson, S. J.; Demchok, J. A.; Felau, I.; Kasapi, M.; Ferguson, M. L.; Hutter, C. M.; Sofia, H. J.; Tarnuzzer, R.; Wang, Z.; Yang, L.; Zenklusen, J. C.; Zhang, J.; Chudamani, S.; Liu, J.; Lolla, L.; Naresh, R.; Pihl, T.; Sun, Q.; Wan, Y.; Wu, Y.; Cho, J.; DeFreitas, T.; Frazer, S.; Gehlenborg, N.; Getz, G.; Heiman, D. I.; Kim, J.; Lawrence, M. S.; Lin, P.; Meier, S.; Noble, M. S.; Saksena, G.; Voet, D.; Zhang, H.; Bernard, B.; Chambwe, N.; Dhankani, V.; Knijnenburg, T.; Kramer, R.; Leinonen, K.; Liu, Y.; Miller, M.; Reynolds, S.; Shmulevich, I.; Thorsson, V.; Zhang, W.; Akbani, R.; Broom, B. M.; Hegde, A. M.; Ju, Z.; Kanchi, R. S.; Korkut, A.; Li, J.; Liang, H.; Ling, S.; Liu, W.; Lu, Y.; Mills, G. B.; Ng, K. S.; Rao, A.; Ryan, M.; Wang, J.; Weinstein, J. N.; Zhang, J.; Abeshouse, A.; Armenia, J.; Chakravarty, D.; Chatila, W. K.; de Bruijn, I.; Gao, J.; Gross, B. E.; Heins, Z. J.; Kundra, R.; La, K.; Ladanyi, M.; Luna, A.; Nissan, M. G.; Ochoa, A.; Phillips, S. M.; Reznik, E.; Sanchez-Vega, F.; Sander, C.; Schultz, N.; Sheridan, R.; Sumer, S. O.; Sun, Y.; Taylor, B. S.; Wang, J.; Zhang, H.; Anur, P.; Peto, M.; Spellman, P.; Benz, C.; Stuart, J. M.; Wong, C. K.; Yau, C.; Hayes, D. N.; Parker, J. S.; Wilkerson, M. D.; Ally, A.; Balasundaram, M.; Bowlby, R.; Brooks, D.; Carlsen, R.; Chuah, E.; Dhalla, N.; Holt, R.; Jones, S. J. M.; Kasaian, K.; Lee, D.; Ma, Y.; Marra, M. A.; Mayo, M.; Moore, R. A.; Mungall, A. J.; Mungall, K.; Robertson, A. G.; Sadeghi, S.; Schein, J. E.; Sipahimalani, P.; Tam, A.; Thiessen, N.; Tse, K.; Wong, T.; Berger, A. C.; Beroukhim, R.; Cibulskis, C.; Gabriel, S. B.; Gao, G. F.; Ha, G.; Meyerson, M.; Schumacher, S. E.; Shih, J.; Kucherlapati, M. H.; Kucherlapati, R. S.; Baylin, S.; Cope, L.; Danilova, L.; Bootwalla, M. S.; Lai, P. H.; Maglinte, D. T.; Van Den Berg, D. J.; Weisenberger, D. J.; Auman, J. T.; Balu, S.; Bodenheimer, T.; Fan, C.; Hoadley, K. A.; Hoyle, A. P.; Jefferys, S. R.; Jones, C. D.; Meng, S.; Mieczkowski, P.

A.; Mose, L. E.; Perou, A. H.; Perou, C. M.; Roach, J.; Shi, Y.; Simons, J. V.; Skelly, T.; Soloway, M. G.; Tan, D.; Veluvolu, U.; Fan, H.; Hinoue, T.; Laird, P. W.; Shen, H.; Zhou, W.; Bellair, M.; Chang, K.; Covington, K.; Creighton, C. J.; Dinh, H.; Doddapaneni, H. V.; Donehower, L. A.; Drummond, J.; Gibbs, R. A.; Glenn, R.; Hale, W.; Han, Y.; Hu, J.; Korchina, V.; Lee, S.; Lewis, L.; Li, W.; Liu, X.; Morgan, M.; Morton, D.; Muzny, D.; Santibanez, J.; Sheth, M.; Shinbrot, E.; Wang, L.; Wang, M.; Wheeler, D. A.; Xi, L.; Zhao, F.; Hess, J.; Appelbaum, E. L.; Bailey, M.; Cordes, M. G.; Ding, L.; Fronick, C. C.; Fulton, L. A.; Fulton, R. S.; Kandoth, C.; Mardis, E. R.; McLellan, M. D.; Miller, C. A.; Schmidt, H. K.; Wilson, R. K.; Crain, D.; Curley, E.; Gardner, J.; Lau, K.; Mallery, D.; Morris, S.; Paulauskis, J.; Penny, R.; Shelton, C.; Shelton, T.; Sherman, M.; Thompson, E.; Yena, P.; Bowen, J.; Gastier-Foster, J. M.; Gerken, M.; Leraas, K. M.; Lichtenberg, T. M.; Ramirez, N. C.; Wise, L.; Zmuda, E.; Corcoran, N.; Costello, T.; Hovens, C.; Carvalho, A. L.; de Carvalho, A. C.; Fregnani, J. H.; Longatto-Filho, A.; Reis, R. M.; Scapulatempo-Neto, C.; Silveira, H. C. S.; Vidal, D. O.; Burnette, A.; Eschbacher, J.; Hermes, B.; Noss, A.; Singh, R.; Anderson, M. L.; Castro, P. D.; Ittmann, M.; Huntsman, D.; Kohl, B.; Le, X.; Thorp, R.; Andry, C.; Duffy, E. R.; Lyadov, V.; Paklina, O.; Setdikova, G.; Shabunin, A.; Tavobilov, M.; McPherson, C.; Warnick, R.; Berkowitz, R.; Cramer, D.; Feltmate, C.; Horowitz, N.; Kibel, A.; Muto, M.; Raut, C. P.; Malykh, A.; Barnholtz-Sloan, J. S.; Barrett, W.; Devine, K.; Fulop, J.; Ostrom, Q. T.; Shimmel, K.; Wolinsky, Y.; Sloan, A. E.; De Rose, A.; Giuliante, F.; Goodman, M.; Karlan, B. Y.; Hagedorn, C. H.; Eckman, J.; Harr, J.; Myers, J.; Tucker, K.; Zach, L. A.; Deyarmin, B.; Hu, H.; Kvecher, L.; Larson, C.; Mural, R. J.; Somiari, S.; Vicha, A.; Zelinka, T.; Bennett, J.; Iacocca, M.; Rabeno, B.; Swanson, P.; Latour, M.; Lacombe, L.; Têtu, B.; Bergeron, A.; McGraw, M.; Staugaitis, S. M.; Chabot, J.; Hibshoosh, H.; Sepulveda, A.; Su, T.; Wang, T.; Potapova, O.; Voronina, O.; Desjardins, L.; Mariani, O.; Roman-Roman, S.; Sastre, X.; Stern, M. H.; Cheng, F.; Signoretti, S.; Berchuck, A.; Bigner, D.; Lipp, E.; Marks, J.; McCall, S.; McLendon, R.; Secord, A.; Sharp, A.; Behera, M.; Brat, D. J.; Chen, A.; Delman, K.; Force, S.; Khuri, F.; Magliocca, K.; Maithel, S.; Olson, J. J.; Owonikoko, T.; Pickens, A.; Ramalingam, S.; Shin, D. M.; Sica, G.; Van Meir, E. G.; Zhang, H.; Eijckenboom, W.; Gillis, A.; Korpershoek, E.; Looijenga, L.; Oosterhuis, W.; Stoop, H.; van Kessel, K. E.; Zwarthoff, E. C.; Calatozzolo, C.; Cuppini, L.; Cuzzubbo, S.; DiMeco, F.; Finocchiaro, G.; Mattei, L.; Perin, A.; Pollo, B.; Chen, C.; Houck, J.; Lohavanichbutr, P.; Hartmann, A.; Stoehr, C.; Stoehr, R.; Taubert, H.; Wach, S.; Wullich, B.; Kycler, W.; Murawa, D.; Wiznerowicz, M.; Chung, K.; Edenfield, W. J.; Martin, J.; Baudin, E.; Bubley, G.; Bueno, R.; De Rienzo, A.; Richards, W. G.; Kalkanis, S.; Mikkelsen, T.; Noushmehr, H.; Scarpace, L.; Girard, N.; Aymerich, M.; Campo, E.; Giné, E.; Guillermo, A. L.; Van Bang, N.; Hanh, P. T.; Phu, B. D.; Tang, Y.; Colman, H.; Evason, K.; Dottino, P. R.; Martignetti, J. A.; Gabra, H.; Juhl, H.; Akeredolu, T.; Stepa, S.; Hoon, D.; Ahn, K.; Kang, K. J.; Beuschlein, F.; Breggia, A.; Birrer, M.; Bell, D.; Borad, M.; Bryce, A. H.; Castle, E.; Chandan, V.; Cheville, J.; Copland, J. A.; Farnell, M.; Flotte, T.; Giama, N.; Ho, T.; Kendrick, M.; Kocher, J. P.; Kopp, K.; Moser, C.; Nagorney, D.; O'Brien, D.; O'Neill, B. P.; Patel, T.; Petersen, G.; Que, F.; Rivera, M.; Roberts, L.; Smallridge, R.; Smyrk, T.; Stanton, M.; Thompson, R. H.; Torbenson, M.; Yang, J. D.; Zhang, L.; Brimo, F.; Ajani, J. A.; Angulo Gonzalez, A. M.; Behrens, C.; Bondaruk, J.; Broaddus, R.; Czerniak, B.; Esmaeli, B.; Fujimoto, J.; Gershenwald, J.; Guo, C.; Lazar, A. J.; Logothetis, C.; Meric-Bernstam, F.; Moran, C.; Ramondetta, L.; Rice, D.; Sood, A.; Tamboli, P.; Thompson, T.; Troncoso, P.; Tsao, A.; Wistuba, I.; Carter, C.; Haydu, L.; Hersey, P.; Jakrot, V.; Kakavand, H.; Kefford, R.; Lee, K.; Long, G.; Mann, G.; Quinn, M.; Saw, R.; Scolyer, R.; Shannon, K.; Spillane, A.; Stretch, J.; Synott, M.; Thompson, J.; Wilmott, J.; Al-Ahmadie, H.; Chan, T. A.; Ghossein, R.; Gopalan, A.; Levine, D. A.; Reuter, V.; Singer, S.; Singh, B.; Tien, N. V.; Broudy, T.; Mirsaidi, C.; Nair, P.; Drwiega, P.; Miller, J.; Smith, J.; Zaren, H.; Park, J. W.; Hung, N. P.; Kebebew, E.; Linehan, W. M.; Metwalli, A. R.; Pacak, K.; Pinto, P. A.; Schiffman, M.; Schmidt, L. S.; Vocke, C. D.; Wentzensen, N.; Worrell, R.; Yang, H.; Moncrieff, M.; Goparaju, C.; Melamed, J.; Pass, H.; Botnariuc, N.; Caraman, I.; Cernat, M.; Chemencedji, I.; Clipca, A.; Doruc, S.; Gorincioi, G.; Mura, S.; Pirtac, M.; Stancul, I.; Tcaciuc, D.; Albert, M.; Alexopoulou, I.; Arnaout, A.; Bartlett, J.; Engel, J.; Gilbert, S.; Parfitt, J.; Sekhon, H.; Thomas, G.; Rassl, D. M.; Rintoul, R. C.; Bifulco, C.; Tamakawa, R.; Urba, W.; Hayward, N.; Timmers, H.; Antenucci, A.; Facciolo, F.; Grazi, G.; Marino, M.; Merola, R.; de Krijger, R.; Gimenez-Roqueplo, A. P.; Piché, A.; Chevalier, S.; McKercher, G.; Birsoy, K.; Barnett, G.; Brewer, C.; Farver, C.; Naska, T.; Pennell, N. A.; Raymond, D.; Schilero, C.; Smolenski, K.; Williams, F.; Morrison, C.; Borgia, J. A.; Liptay, M. J.; Pool, M.; Seder, C. W.; Junker, K.; Omberg, L.; Dinkin, M.; Manikhas, G.; Alvaro, D.; Bragazzi, M. C.; Cardinale, V.; Carpino, G.; Gaudio, E.; Chesla, D.; Cottingham, S.; Dubina, M.; Moiseenko, F.; Dhanasekaran, R.; Becker, K. F.; Janssen, K. P.; Slotta-Huspenina, J.; Abdel-Rahman, M. H.; Aziz, D.; Bell, S.; Cebulla, C. M.; Davis, A.; Duell, R.; Elder, J. B.; Hilty, J.; Kumar, B.; Lang, J.; Lehman, N. L.; Mandt, R.; Nguyen, P.; Pilarski, R.; Rai, K.; Schoenfield, L.; Senecal, K.; Wakely, P.; Hansen, P.; Lechan, R.; Powers, J.; Tischler, A.; Grizzle, W. E.; Sexton, K. C.; Kastl, A.; Henderson, J.; Porten, S.; Waldmann, J.; Fassnacht, M.; Asa, S. L.; Schadendorf, D.; Couce, M.; Graefen, M.; Huland, H.; Sauter, G.; Schlomm, T.; Simon, R.; Tennstedt, P.; Olabode, O.; Nelson, M.; Bathe, O.; Carroll, P. R.; Chan, J. M.; Disaia, P.; Glenn, P.; Kelley, R. K.; Landen, C. N.; Phillips, J.; Prados, M.; Simko, J.; Smith-McCune, K.; VandenBerg, S.; Roggin, K.; Fehrenbach, A.; Kendler, A.; Sifri, S.; Steele, R.; Jimeno, A.; Carey, F.; Forgie, I.; Mannelli, M.; Carney, M.; Hernandez, B.; Campos, B.; Herold-Mende, C.; Jungk, C.; Unterberg, A.; von Deimling, A.; Bossler, A.; Galbraith, J.; Jacobus, L.; Knudson, M.; Knutson, T.; Ma, D.; Milhem, M.; Sigmund, R.; Godwin, A. K.; Madan, R.; Rosenthal, H. G.; Adebamowo, C.; Adebamowo, S. N.; Boussioutas, A.; Beer, D.; Giordano, T.; Mes-Masson, A. M.; Saad, F.; Bocklage, T.; Landrum, L.; Mannel, R.; Moore, K.; Moxley, K.; Postier, R.; Walker, J.; Zuna, R.; Feldman, M.; Valdivieso, F.; Dhir, R.; Luketich, J.; Mora Pinero, E. M.; Quintero-Aguilo, M.; Carlotti, C. G.; Dos Santos, J. S.; Kemp, R.; Sankarankuty, A.; Tirapelli, D.; Catto, J.; Agnew, K.; Swisher, E.; Creaney, J.; Robinson, B.; Shelley, C. S.; Godwin, E. M.; Kendall, S.; Shipman, C.; Bradford, C.; Carey, T.; Haddad, A.; Moyer, J.; Peterson, L.; Prince, M.; Rozek, L.; Wolf, G.; Bowman, R.; Fong, K. M.; Yang, I.; Korst, R.; Rathmell, W. K.; Fantacone-Campbell, J. L.; Hooke, J. A.; Kovatich, A. J.; Shriver, C. D.; DiPersio, J.; Drake, B.; Govindan, R.; Heath, S.; Ley, T.; Van Tine, B.; Westervelt, P.; Rubin, M. A.; Lee, J. Il; Aredes, N. D.; Mariamidze, A. Pan-Cancer Alterations of the MYC Oncogene and Its Proximal Network across the Cancer Genome Atlas. *Cell Syst.* **2018**, *6* (3), 282−300.

(16) Duffy, M. J.; O'Grady, S.; Tang, M.; Crown, J. MYC as a Target for Cancer Treatment. *Cancer Treat. Rev.* **2021**, *94*, No. 102154.

(17) Blackwood, E. M.; Eisenman, R. N. Max: A Helix-Loop-Helix Zipper Protein That Forms a Sequence-Specific DNA-Binding Complex with Myc. *Science (80-.)* **1991**, *251* (4998), 1211−1217.

(18) Amati, B.; Brooks, M. W.; Levy, N.; Littlewood, T. D.; Evan, G. I.; Land, H. Oncogenic Activity of the C-Myc Protein Requires Dimerization with Max. *Cell* **1993**, *72* (2), 233−245.

(19) Knoepfler, P. S.; Zhang, X. Y.; Cheng, P. F.; Gafken, P. R.; McMahon, S. B.; Eisenman, R. N. Myc Influences Global Chromatin Structure. *EMBO J.* **2006**, *25* (12), 2723−2734.

(20) Beaulieu, M. E.; Castillo, F.; Soucek, L. Structural and Biophysical Insights into the Function of the Intrinsically Disordered Myc Oncoprotein. *Cells* **2020**, *9* (4), 1038.

(21) Jin, F.; Yu, C.; Lai, L.; Liu, Z. Ligand Clouds around Protein Clouds: A Scenario of Ligand Binding with Intrinsically Disordered Proteins. *PLoS Comput. Biol.* **2013**, *9* (10), No. e1003249.

(22) Soucek, L.; Whitfield, J.; Martins, C. P.; Finch, A. J.; Murphy, D. J.; Sodir, N. M.; Karnezis, A. N.; Swigart, L. B.; Nasi, S.; Evan, G. I. Modelling Myc Inhibition as a Cancer Therapy. *Nature* **2008**, *455* (7213), 679−683.

(23) Horiuchi, D.; Anderton, B.; Goga, A. Taking on Challenging Targets: Making MYC Druggable. *Am. Soc. Clin. Oncol. Educ. book. Am. Soc. Clin. Oncol. Annu. Meet.* **2014**, *34* (1), e497−e502.

https://doi.org/10.1021/acsomega.4c10201
ACS Omega 2024, 9, 50844−50858

(24) Jeong, K. C.; Ahn, K. O.; Yang, C. H. Small-Molecule Inhibitors of c-Myc Transcriptional Factor Suppress Proliferation and Induce Apoptosis of Promyelocytic Leukemia Cell via Cell Cycle Arrest. *Mol. Biosyst.* **2010**, *6* (8), 1503−1509.
(25) Llombart, V.; Mansour, M. R. Therapeutic Targeting of "Undruggable" MYC. *EBioMedicine.* **2022**, *75*, No. 103756.
(26) Lin, C. Y.; Lovén, J.; Rahl, P. B.; Paranal, R. M.; Burge, C. B.; Bradner, J. E.; Lee, T. I.; Young, R. A. Transcriptional Amplification in Tumor Cells with Elevated C-Myc. *Cell* **2012**, *151* (1), 56−67.
(27) Dhanasekaran, R.; Baylot, V.; Kim, M.; Kuruvilla, S.; Bellovin, D. I.; Adeniji, N.; Rajan, K. D. A.; Lai, I.; Gabay, M.; Tong, L.; Krishnan, M.; Park, J.; Hu, T.; Barbhuiya, M. A.; Gentles, A. J.; Kannan, K.; Tran, P. T.; Felsher, D. W. MYC and Twist1 Cooperate to Drive Metastasis by Eliciting Crosstalk between Cancer and Innate Immunity. *eLife* **2020**, *9*, No. e50731.
(28) Struntz, N. B.; Chen, A.; Deutzmann, A.; Wilson, R. M.; Stefan, E.; Evans, H. L.; Ramirez, M. A.; Liang, T.; Caballero, F.; Wildschut, M. H. E.; Neel, D. V.; Freeman, D. B.; Pop, M. S.; McConkey, M.; Muller, S.; Curtin, B. H.; Tseng, H.; Frombach, K. R.; Butty, V. L.; Levine, S. S.; Feau, C.; Elmiligy, S.; Hong, J. A.; Lewis, T. A.; Vetere, A.; Clemons, P. A.; Malstrom, S. E.; Ebert, B. L.; Lin, C. Y.; Felsher, D. W.; Koehler, A. N. Stabilization of the Max Homodimer with a Small Molecule Attenuates Myc-Driven Transcription. *Cell Chem. Biol.* **2019**, *26* (5), 711−723.
(29) Castell, A.; Yan, Q.; Fawkner, K.; Hydbring, P.; Zhang, F.; Verschut, V.; Franco, M.; Zakaria, S. M.; Bazzar, W.; Goodwin, J.; Zinzalla, G.; Larsson, L. G. A Selective High Affinity MYC-Binding Compound Inhibits MYC:MAX Interaction and MYC-Dependent Tumor Cell Proliferation. *Sci. Rep.* **2018**, *8*, 10064.
(30) Jeong, K. C.; Kim, K. T.; Seo, H. H.; Shin, S. P.; Ahn, K. O.; Ji, M. J.; Park, W. S.; Kim, I. H.; Lee, S. J.; Seo, H. K. Intravesical Instillation of C-MYC Inhibitor KSI-3716 Suppresses Orthotopic Bladder Tumor Growth. *J. Urol.* **2014**, *191* (2), 510−518.
(31) Seo, H. K.; Shin, S. P.; Jung, N. R.; Kwon, W. A.; Jeong, K. C.; Lee, S. J. The Establishment of a Growth-Controllable Orthotopic Bladder Cancer Model through the down-Regulation of c-Myc Expression. *Oncotarget* **2017**, *8* (31), 50500−50509.
(32) Hsu, T. Y. T.; Simon, L. M.; Neill, N. J.; Marcotte, R.; Sayad, A.; Bland, C. S.; Echeverria, G. V.; Sun, T.; Kurley, S. J.; Tyagi, S.; Karlin, K. L.; Dominguez-Vidaña, R.; Hartman, J. D.; Renwick, A.; Scorsone, K.; Bernardi, R. J.; Skinner, S. O.; Jain, A.; Orellana, M.; Lagisetti, C.; Golding, I.; Jung, S. Y.; Neilson, J. R.; Zhang, X. H. F.; Cooper, T. A.; Webb, T. R.; Neel, B. G.; Shaw, C. A.; Westbrook, T. F. The Spliceosome Is a Therapeutic Vulnerability in MYC-Driven Cancer. *Nature* **2015**, *525* (7569), 384−388.
(33) Thomas, L. R.; Wang, Q.; Grieb, B. C.; Phan, J.; Foshage, A. M.; Sun, Q.; Olejniczak, E. T.; Clark, T.; Dey, S.; Lorey, S.; Alicie, B.; Howard, G. C.; Cawthon, B.; Ess, K. C.; Eischen, C. M.; Zhao, Z.; Fesik, S. W.; Tansey, W. P. Interaction with WDR5 Promotes Target Gene Recognition and Tumorigenesis by MYC. *Mol. Cell* **2015**, *58* (3), 440−452.
(34) Liu, H.; Ai, J.; Shen, A.; Chen, Y.; Wang, X.; Peng, X.; Chen, H.; Shen, Y.; Huang, M.; Ding, J.; Geng, M. C-Myc Alteration Determines the Therapeutic Response to FGFR Inhibitors. *Clin. cancer Res.* **2017**, *23* (4), 974−984.
(35) Sliwoski, G.; Kothiwale, S.; Meiler, J.; Lowe, E. W. Computational Methods in Drug Discovery. *Pharmacol. Rev.* **2014**, *66* (1), 334−395.
(36) Lin, X.; Li, X.; Lin, X. A Review on Applications of Computational Methods in Drug Screening and Design. *Mol.* **2020**, *25* (6), 1375.
(37) Jiang, H.; Bower, K. E.; Beuscher, A. E., IV; Zhou, B.; Bobkov, A. A.; Olson, A. J.; Vogt, P. K. Stabilizers of the Max Homodimer Identified in Virtual Ligand Screening Inhibit Myc Function. *Mol. Pharmacol.* **2009**, *76* (3), 491−502.
(38) Yu, C.; Niu, X.; Jin, F.; Liu, Z.; Jin, C.; Lai, L. Structure-Based Inhibitor Design for the Intrinsically Disordered Protein c-Myc. *Sci. Rep.* **2016**, *6*, 22298.
(39) Carabet, L. A.; Rennie, P. S.; Cherkasov, A. Therapeutic Inhibition of Myc in Cancer. Structural Bases and Computer-Aided Drug Discovery Approaches. *Int. J. Mol. Sci.* **2019**, *20* (1), 120.
(40) Singh, A.; Kumar, P.; Sarvagalla, S.; Bharadwaj, T.; Nayak, N.; Coumar, M. S.; Giri, R.; Garg, N. Functional Inhibition of C-Myc Using Novel Inhibitors Identified through "Hot Spot" Targeting. *J. Biol. Chem.* **2022**, *298* (5), No. 101898.
(41) Zhou, M.; Boulos, J. C.; Omer, E. A.; Klauck, S. M.; Efferth, T. Modes of Action of a Novel C-MYC Inhibiting 1,2,4-Oxadiazole Derivative in Leukemia and Breast Cancer Cells. *Molecules* **2023**, *28* (15), 5658.
(42) Lu, Y.; Zhou, J.; Hu, T.; Zhang, Y.; Su, P.; Wang, J.; Gao, W.; Huang, L. A Multifunctional Oxidosqualene Cyclase from Tripterygium Regelii That Produces Both α- and β-Amyrin. *RSC Adv.* **2018**, *8* (42), 23516−23521.
(43) Zheng, C.; Rangsinth, P.; Shiu, P. H. T.; Wang, W.; Li, R.; Li, J.; Kwan, Y. W.; Leung, G. P. H. A Review on the Sources, Structures, and Pharmacological Activities of Lucidenic Acids. *Molecules* **2023**, *28* (4), 1756.
(44) Du, Y.; Tian, L.; Wang, Y.; Li, Z.; Xu, Z. Chemodiversity, Pharmacological Activity, and Biosynthesis of Specialized Metabolites from Medicinal Model Fungi Ganoderma Lucidum. *Chin. Med.* **2024**, *19*, 51.
(45) Xia, Q.; Zhang, H.; Sun, X.; Zhao, H.; Wu, L.; Zhu, D.; Yang, G.; Shao, Y.; Zhang, X.; Mao, X.; Zhang, L.; She, G. A Comprehensive Review of the Structure Elucidation and Biological Activity of Triterpenoids from Ganoderma Spp. *Molecules* **2014**, *19* (11), 17478−17535.
(46) Galappaththi, M. C. A.; Patabendige, N. M.; Premarathne, B. M.; Hapuarachchi, K. K.; Tibpromma, S.; Dai, D. Q.; Suwannarach, N.; Rapior, S.; Karunarathna, S. C. A Review of Ganoderma Triterpenoids and Their Bioactivities. *Biomolecules.* **2023**, *13* (1), 24.
(47) Liu, C.; Song, X.; Li, Y.; Ding, C.; Li, X.; Dan, L.; Xu, H.; Zhang, D. A Comprehensive Review on the Chemical Composition, Pharmacology and Clinical Applications of Ganoderma. *Am. J. Chin. Med.* **2023**, *51* (8), 1983−2040.
(48) Ma, Q.; Zhang, S.; Yang, L.; Xie, Q.; Dai, H.; Yu, Z.; Zhao, Y. Lanostane Triterpenoids and Ergostane Steroids from Ganoderma Luteomarginatum and Their Cytotoxicity. *Mol.* **2022**, *27* (20), 6989.
(49) Su, H. G.; Zhou, Q. M.; Guo, L.; Huang, Y. J.; Peng, C.; Xiong, L. Lanostane Triterpenoids from Ganoderma Luteomarginatum and Their Cytotoxicity against Four Human Cancer Cell Lines. *Phytochemistry* **2018**, *156*, 89−95.
(50) Yao, J. N.; Chen, L.; Tang, Y.; Chen, H. P.; Zhao, Z. Z.; Li, Z. H.; Feng, T.; Liu, J. K. Lanostane Triterpenoids from Fruiting Bodies of Basidiomycete Stereum Sp., Structures and Biological Activities. *J. Antibiot. (Tokyo)* **2017**, *70* (12), 1104−1111.
(51) Shi, J. X.; Chen, G. Y.; Sun, Q.; Meng, S. Y.; Chi, W. Q. Antimicrobial Lanostane Triterpenoids from the Fruiting Bodies of Ganoderma Applanatum. *J. Asian Nat. Prod. Res.* **2022**, *24* (11), 1001−1007.
(52) Peng, G.; Xiong, C.; Zeng, X.; Jin, Y.; Huang, W. Exploring Nutrient Profiles, Phytochemical Composition, and the Antiproliferative Activity of *Ganoderma lucidum* and *Ganoderma leucocontextum*: A Comprehensive Comparative Study. *Foods* **2024**, *13*, 614.
(53) Xu, Q.; Sheng, C. Y. Lanostane Triterpenoids from the Fruiting Bodies of Ganoderma Hainanense and Their Cytotoxic Activity. *J. Asian Nat. Prod. Res.* **2023**, *25* (4), 342−348.
(54) Montenegro, R. C.; Jimenez, P. C.; Feio Farias, R. A.; Andrade-Neto, M.; Silva Bezerra, F.; Moraes, M. E. A.; Odorico de Moraes, M.; Pessoa, C.; Costa-Lotufo, L. V. Cytotoxic Activity of Pisosterol, a Triterpene Isolated from Pisolithus Tinctorius (Mich.: Pers.) Coker & Couch, 1928. *Z. Naturforsch. C.* **2004**, *59* (7−8), 519−522.
(55) Montenegro, R. C.; de Vasconcellos, M. C.; Silva Bezerra, F.; Andrade-Neto, M.; Pessoa, C.; de Moraes, M. O.; Costa-Lotufo, L. V. Pisosterol Induces Monocytic Differentiation in HL-60 Cells. *Toxicol. In Vitro* **2007**, *21* (5), 795−800.
(56) Ferreira, W. A. S.; Burbano, R. R.; Pessoa, C. D. Ó.; Harada, M. L.; do Nascimento Borges, B.; de Oliveira, E. H. C. Pisosterol Induces

https://doi.org/10.1021/acsomega.4c10201
ACS Omega 2024, 9, 50844−50858

G2/M Cell Cycle Arrest and Apoptosis via the ATM/ATR Signaling Pathway in Human Glioma Cells. *Anticancer Agents Med. Chem.* **2020**, *20* (6), 734−750.
(57) Silva, T. C. R.; Lima, P. D. L.; Bahia, M. O.; Khayat, A. S.; Bezerra, F. S.; Andrade-Neto, M.; Seabra, A. D.; Pontes, T. B.; Moraes, M. O.; Montenegro, R. C.; Costa-Lotufo, L. V.; Pessoa, C.; Pinto, G. R.; Burbano, R. R. Pisosterol Induces Interphase Arrest in HL60 Cells with C-MYC Amplification. *Hum. Exp. Toxicol.* **2010**, *29* (3), 235−240.
(58) Pereira, E. L. R.; Lima, P. D. L.; Khayat, A. S.; Bahia, M. O.; Bezerra, F. S.; Andrade-Neto, M.; Montenegro, R. C.; Pessoa, C.; Costa-Lotufo, L. V.; Moraes, M. O.; Yoshioka, F. K. N.; Pinto, G. R.; Burbano, R. R. Inhibitory Effect of Pisosterol on Human Glioblastoma Cell Lines with C-MYC Amplification. *J. Appl. Toxicol.* **2011**, *31* (6), 554−560.
(59) Kar, S.; Leszczynski, J. Open Access in Silico Tools to Predict the ADMET Profiling of Drug Candidates. *Expert Opin. Drug Discov.* **2020**, *15* (12), 1473−1487.
(60) Jambhekar, S. S.; Breen, P. J. Drug Dissolution: Significance of Physicochemical Properties and Physiological Conditions. *Drug Discov. Today* **2013**, *18* (23−24), 1173−1184.
(61) Azman, M.; Sabri, A. H.; Anjani, Q. K.; Mustaffa, M. F.; Hamid, K. A. Intestinal Absorption Study: Challenges and Absorption Enhancement Strategies in Improving Oral Drug Delivery. *Pharm.* **2022**, *15* (8), 975.
(62) Stavropoulou, E.; Pircalabioru, G. G.; Bezirtzoglou, E. The Role of Cytochromes P450 in Infection. *Front. Immunol.* **2018**, *9*, 89.
(63) Lagares, L. M.; Minovski, N.; Novič, M. Multiclass Classifier for P-Glycoprotein Substrates, Inhibitors, and Non-Active Compounds. *Molecules* **2019**, *24* (10), 2006.
(64) Yang, P. C.; Demarco, K. R.; Aghasafari, P.; Jeng, M. T.; Dawson, J. R. D.; Bekker, S.; Noskov, S. Y.; Yarov-Yarovoy, V.; Vorobyov, I.; Clancy, C. E. A Computational Pipeline to Predict Cardiotoxicity: From the Atom to the Rhythm. *Circ. Res.* **2020**, *126* (8), 947−964.
(65) He, S.; Ye, T.; Wang, R.; Zhang, C.; Zhang, X.; Sun, G.; Sun, X. An In Silico Model for Predicting Drug-Induced Hepatotoxicity. *Int. J. Mol. Sci.* **2019**, *20* (8), 1897.
(66) Wu, D.; Chen, Q.; Chen, X.; Han, F.; Chen, Z.; Wang, Y. The Blood-Brain Barrier: Structure, Regulation, and Drug Delivery. *Signal Transduction Targeted Ther.* **2023**, *8*, 217.
(67) Kim, K. H.; Moon, E.; Choi, S. U.; Kim, S. Y.; Lee, K. R. Lanostane triterpenoids from the mushroom Naematoloma fasciculare. *J. Nat. Prod.* **2013**, *76* (5), 845−851.
(68) Upadhyay, M.; Shrivastava, B.; Jain, A.; Kidwai, M.; Kumar, S.; Gomes, J.; Goswami, D. G.; Panda, A. K.; Kuhad, R. C. Production of ganoderic acid by *Ganoderma lucidum* RCKB-2010 and its therapeutic potential. *Ann. Microbiol.* **2014**, *64*, 839−846.
(69) Li, Q.; Zheng, Y.; Fu, A.; Wei, M.; Kang, X.; Chen, C.; Zhu, H.; Zhang, Y. 30-norlanostane triterpenoids and steroid derivatives from the endophytic fungus Aspergillus nidulans. *Phytochemistry* **2022**, *201*, No. 113257.
(70) Li, J. C.; Li, S. Y.; Tang, J. X.; Liu, D.; Feng, X. Y.; Rao, K. R.; Zhao, X. D.; Li, H. M.; Li, R. T. Triterpenoids, steroids and other constituents from Euphorbia kansui and their anti-inflammatory and anti-tumor properties. *Phytochemistry* **2022**, *204*, No. 113449.
(71) Lee, D. J.; Hong, S. M.; Yoon, D. H.; Ham, S. L.; Kim, J.; Kim, S. Y.; Choi, S. U.; Kim, C. S.; Lee, K. R. Triterpenoids from the leaves of Abies koreana and their biological activities. *Phytochemistry* **2023**, *208*, No. 113594.
(72) Kikuchi, T.; Matsuda, S.; Kadota, S.; Murai, Y.; Ogita, Z. Ganoderic acid D, E, F, and H and lucidenic acid D, E, and F, new triterpenoids from ganoderma lucidum. *Chem. Pharm. Bull.* **1985**, *33* (6), 2624−2627.
(73) Wei, J. C.; Wang, Y. X.; Dai, R.; Tian, X. G.; Sun, C. P.; Ma, X. C.; Jia, J. M.; Zhang, B. J.; Huo, X. K.; Wang, C. C27-Nor Lanostane Triterpenoids of the Fungus Ganoderma Lucidum and Their Inhibitory Effects on Acetylcholinesteras. *Phytochem. Lett.* **2017**, *20*, 263−268.
(74) Lee, I. S.; Ahn, B. R.; Choi, J. S.; Hattori, M.; Min, B.; Bae, K. H. Selective Cholinesterase Inhibition by Lanostane Triterpenes from Fruiting Bodies of Ganoderma Lucidum. *Bioorg. Med. Chem. Lett.* **2011**, *21* (21), 6603−6607.
(75) Zhang, W.; Tao, J.; Yang, X.; Yang, Z.; Zhang, L.; Liu, H.; Wu, K.; Wu, J. Antiviral Effects of Two Ganoderma Lucidum Triterpenoids against Enterovirus 71 Infection. *Biochem. Biophys. Res. Commun.* **2014**, *449* (3), 307−312.
(76) Wang, K.; Bao, L.; Xiong, W.; Ma, K.; Han, J.; Wang, W.; Yin, W.; Liu, H. Lanostane Triterpenes from the Tibetan Medicinal Mushroom Ganoderma Leucocontextum and Their Inhibitory Effects on HMG-CoA Reductase and α-Glucosidase. *J. Nat. Prod.* **2015**, *78* (8), 1977−1989.
(77) Fatmawati, S.; Shimizu, K.; Kondo, R. Ganoderic Acid Df, a New Triterpenoid with Aldose Reductase Inhibitory Activity from the Fruiting Body of Ganoderma Lucidum. *Fitoterapia* **2010**, *81* (8), 1033−1036.
(78) Kikuchi, T.; Kanoumi, A.; Kadota, S.; Murai, Y.; Tsubono, K.; Ogita, Z. Constitutents of the Fungus Ganoderma Lucidum (FR.) KARST. I.: Structures of Ganoderic Acids C2, E, I, and K, Lucidenic Acid F and Related Compounds. *Chem. Pharm. Bull.* **1986**, *34* (9), 3695−3712.
(79) Akihisa, T.; Nakamura, Y.; Tagata, M.; Tokuda, H.; Yasukawa, K.; Uchiyama, E.; Suzuki, T.; Kimura, Y. Anti-Inflammatory and Anti-Tumor-Promoting Effects of Triterpene Acids and Sterols from the Fungus Ganoderma Lucidum. *Chem. Biodivers.* **2007**, *4* (2), 224−231.
(80) Liu, L. Y.; Yan, Z.; Kang, J.; Chen, R. Y.; Yu, D. Q. Three New Triterpenoids from Ganoderma Theaecolum. *J. Asian Nat. Prod. Res.* **2017**, *19* (9), 847−853.
(81) Hasegawa, S.; Miura, T.; Kaneko, N.; Hirose, Y.; Iitaka, Y. Further New Rearranged Lanostanoids from the Seeds of Abies Mariesii and A. *Firma. Tetrahedron* **1987**, *43* (8), 1775−1784.
(82) Li, Y. T.; Zhang, Z.; Feng, Y.; Cheng, Y.; Li, S.; Li, C.; Tian, L. W. Cardioprotective 22-Hydroxylanostane Triterpenoids from the Fruiting Bodies of Phellinus Igniarius. *Phytochemistry.* **2021**, *191*, No. 112907.
(83) Yao, R.; Zhang, M.; Zhou, J.; Liu, L.; Zhang, Y.; Gao, J.; Xu, K. Novel Dual-Targeting c-Myc Inhibitor D347−2761 Represses Myeloma Growth via Blocking c-Myc/Max Heterodimerization and Disturbing Its Stability. *Cell Commun. Signaling* **2022**, *20* (1), 73.
(84) Singh, A.; Kumar, A.; Kumar, P.; Nayak, N.; Bhardwaj, T.; Giri, R.; Garg, N. A Novel Inhibitor L755507 Efficiently Blocks C-Myc-MAX Heterodimerization and Induces Apoptosis in Cancer Cells. *J. Biol. Chem.* **2021**, *297* (1), No. 100903.
(85) Knapp, B.; Frantal, S.; Cibena, M.; Schreiner, W.; Bauer, P. Is an Intuitive Convergence Definition of Molecular Dynamics Simulations Solely Based on the Root Mean Square Deviation Possible? *J. Comput. Biol.* **2011**, *18* (8), 997−1005.
(86) Martínez, L. Automatic Identification of Mobile and Rigid Substructures in Molecular Dynamics Simulations and Fractional Structural Fluctuation Analysis. *PLOS ONE* **2015**, *10*, No. e0119264.
(87) Fuglebakk, E.; Echave, J.; Reuter, N. Measuring and Comparing Structural Fluctuation Patterns in Large Protein Datasets. *Bioinforma.* **2012**, *28* (19), 2431−2440.
(88) Bagewadi, Z. K.; Khan, T. M. Y; Gangadharappa, B.; Kamalapurkar, A.; Shamsudeen, S. M.; Yaraguppi, D. A. Molecular dynamics and simulation analysis against superoxide dismutase (SOD) target of *Micrococcus luteus* with secondary metabolites from *Bacillus licheniformis* recognized by genome mining approach. *Saudi J. Biol. Sci.* **2023**, *30* (9), No. 103753.
(89) Lobanov, M. Y.; Bogatyreva, N. S.; Galzitskaya, O. V. Radius of gyration as an indicator of protein structure compactness. *Mol. Biol.* **2008**, *42*, 623−628.
(90) Amperayani, K. R.; Varadhi, G.; Oruganti, B.; Parimi, U. D. Molecular Dynamics and Absolute Binding Free Energy Studies of Piperine Derivatives as Potential Inhibitors of SARS-CoV-2 Main Protease. *J. Biomol. Struct. Dyn.* **2023**, *41* (23), 13696−13706.
(91) Menéndez, C. A.; Accordino, S. R.; Gerbino, D. C.; Appignanesi, G. A. Hydrogen Bond Dynamic Propensity Studies for

https://doi.org/10.1021/acsomega.4c10201
ACS Omega 2024, 9, 50844−50858

Protein Binding and Drug Design. *PLoS One.* **2016**, *11* (10), No. e0165767.
(92) Humphrey, W.; Dalke, A.; Schulten, K. VMD: Visual Molecular Dynamics. *J. Mol. Graph.* **1996**, *14* (1), 33−38.
(93) Yalazan, H.; Koç, D.; Aydın Kose, F.; Fandaklı, S.; Tüzün, B.; Akgül, M. İ.; Sadeghian, N.; Taslimi, P.; Kantekin, H. Design, Syntheses, Theoretical Calculations, MM-GBSA, Potential Anti-Cancer and Enzyme Activities of Novel Schiff Base Compounds. *J. Biomol. Struct. Dyn.* **2023**, *42*, 13100−13113.
(94) Wan, S.; Bhati, A. P.; Zasada, S. J.; Coveney, P. V. Rapid, Accurate, Precise and Reproducible Ligand-Protein Binding Free Energy Prediction. *Interface Focus.* **2020**, *10* (6), 20200007.
(95) Montenegro, R. C.; Feio Farias, R. A.; Pinho Pereira, M. R.; Alves, A. P. N. N.; Bezerra, F. S.; Andrade-Neto, M.; Pessoa, C.; De Moraes, M. O.; Costa-Lotufo, L. V. Antitumor Activity of Pisosterol in Mice Bearing with S180 Tumor. *Biol. Pharm. Bull.* **2008**, *31* (3), 454−457.
(96) Cousins, K. R. Computer Review of ChemDraw Ultra 12.0. *J. Am. Chem. Soc.* **2011**, *133* (21), 8388.
(97) Hanwell, M. D.; Curtis, D. E.; Lonie, D. C.; Vandermeerschd, T.; Zurek, E.; Hutchison, G. R. Avogadro: An Advanced Semantic Chemical Editor, Visualization, and Analysis Platform. *J. Cheminform.* **2012**, *4*, 17.
(98) O'Boyle, N. M.; Banck, M.; James, C. A.; Morley, C.; Vandermeersch, T.; Hutchison, G. R. Open Babel: An Open Chemical Toolbox. *J. Cheminf.* **2011**, *3* (1), 33.
(99) Berman, H. M.; Westbrook, J.; Feng, Z.; Gilliland, G.; Bhat, T. N.; Weissig, H.; Shindyalov, I. N.; Bourne, P. E. The Protein Data Bank. *Nucleic Acids Res.* **2000**, *28* (1), 235−242.
(100) Nair, S. K.; Burley, S. K. X-Ray Structures of Myc-Max and Mad-Max Recognizing DNA: Molecular Bases of Regulation by Proto-Oncogenic Transcription Factors. *Cell* **2003**, *112* (2), 193−205.
(101) Rigsby, R. E.; Parker, A. B. Using the PyMOL Application to Reinforce Visual Understanding of Protein Structure. *Biochem. Mol. Biol. Educ.* **2016**, *44* (5), 433−437.
(102) Dolinsky, T. J.; Nielsen, J. E.; McCammon, J. A.; Baker, N. A. PDB2PQR: An Automated Pipeline for the Setup of Poisson-Boltzmann Electrostatics Calculations. *Nucleic Acids Res.* **2004**, *32* (Issue suppl_2), W665−W667.
(103) Laskowski, R. A.; MacArthur, M. W.; Moss, D. S.; Thornton, J. M. PROCHECK: A Program to Check the Stereochemical Quality of Protein Structures. *J. Appl. Crystallogr.* **1993**, *26* (2), 283−291.
(104) Abraham, M. J.; Murtola, T.; Schulz, R.; Páll, S.; Smith, J. C.; Hess, B.; Lindah, E. GROMACS: High Performance Molecular Simulations through Multi-Level Parallelism from Laptops to Supercomputers. *SoftwareX* **2015**, *1-2*, 19−25.
(105) Conev, A.; Rigo, M. M.; Devaurs, D.; Fonseca, A. F.; Kalavadwala, H.; de Freitas, M. V.; Clementi, C.; Zanatta, G.; Antunes, D. A.; Kavraki, L. E. EnGens: A Computational Framework for Generation and Analysis of Representative Protein Conformational Ensembles. *Briefings Bioinf.* **2023**, *24* (4), 1−11.
(106) Xu, Y.; Wang, S.; Hu, Q.; Gao, S.; Ma, X.; Zhang, W.; Shen, Y.; Chen, F.; Lai, L.; Pei, J. CavityPlus: A Web Server for Protein Cavity Detection with Pharmacophore Modelling, Allosteric Site Identification and Covalent Ligand Binding Ability Prediction. *Nucleic Acids Res.* **2018**, *46* (W1), W374−W379.
(107) Eberhardt, J.; Santos-Martins, D.; Tillack, A. F.; Forli, S. AutoDock Vina 1.2.0: New Docking Methods, Expanded Force Field, and Python Bindings. *J. Chem. Inf. Model.* **2021**, *61* (8), 3891−3898.
(108) Daina, A.; Michielin, O.; Zoete, V. SwissADME: A Free Web Tool to Evaluate Pharmacokinetics, Drug-Likeness and Medicinal Chemistry Friendliness of Small Molecules. *Sci. Rep.* **2017**, *7* (1), 42717.
(109) Lipinski, C. A.; Lombardo, F.; Dominy, B. W.; Feeney, P. J. Experimental and Computational Approaches to Estimate Solubility and Permeability in Drug Discovery and Development Settings. *Adv. Drug Deliv. Rev.* **2001**, *46* (1−3), 3−26.
(110) Veber, D. F.; Johnson, S. R.; Cheng, H. Y.; Smith, B. R.; Ward, K. W.; Kopple, K. D. Molecular Properties That Influence the Oral Bioavailability of Drug Candidates. *J. Med. Chem.* **2002**, *45* (12), 2615−2623.
(111) Dong, J.; Wang, N. N.; Yao, Z. J.; Zhang, L.; Cheng, Y.; Ouyang, D.; Lu, A. P.; Cao, D. S. ADMETlab: A Platform for Systematic ADMET Evaluation Based on a Comprehensively Collected ADMET Database. *J. Cheminf.* **2018**, *10* (1), 29.
(112) Smardz, P.; Anila, M. M.; Rogowski, P.; Li, M. S.; Różycki, B.; Krupa, P. Protocols for Multi-Scale Molecular Dynamics Simulations: A Comparative Study for Intrinsically Disordered Amyloid Beta in Amber & Gromacs on CPU & GPU. *BioRxiv*. 2024.
(113) Hornak, V.; Abel, R.; Okur, A.; Strockbine, B.; Roitberg, A.; Simmerling, C. Comparison of Multiple Amber Force Fields and Development of Improved Protein Backbone Parameters. *Proteins* **2006**, *65* (3), 712−725.
(114) Sousa da Silva, A. W.; Vranken, W. F. ACPYPE - AnteChamber PYthon Parser InterfacE. *BMC Res. Notes* **2012**, *5*, 367.
(115) Kagami, L.; Wilter, A.; Diaz, A.; Vranken, W.; Elofsson, A. The ACPYPE Web Server for Small-Molecule MD Topology Generation. *Bioinformatics* **2023**, *39* (6), No. btad350.
(116) Valdés-Tresanco, M. S.; Valdés-Tresanco, M. E.; Valiente, P. A.; Moreno, E. Gmx_MMPBSA: A New Tool to Perform End-State Free Energy Calculations with GROMACS. *J. Chem. Theory Comput.* **2021**, *17* (10), 6281−6291.

https://doi.org/10.1021/acsomega.4c10201
ACS Omega 2024, 9, 50844−50858